2016

Robust Nickel Catalysts Supported By Biaryl-Bridged Pyridyl-N-Heterocyclic Carbenes For Carbon Dioxide Reduction To Value-Added Products

Hunter Allen Dulaney
University of Mississippi

ROBUST NICKEL CATALYSTS SUPPORTED BY BIARYL-BRIDGED PYRIDYL-*N*-HETEROCYCLIC CARBENES FOR CARBON DIOXIDE REDUCTION TO VALUE-ADDED PRODUCTS

A Thesis
Presented in partial fulfillment of requirements
For the degree of Master of Science
The University of Mississippi

by

HUNTER ALLEN DULANEY

August 2016

ABSTRACT

Carbon dioxide is a greenhouse gas, but also represents a readily accessible C1 feedstock for conversion to solar fuels and value-added chemicals. However, CO_2 is relatively inert and very negative voltages or strong chemical reductants are common for its conversion. An additional challenge lies in achieving these reactions in water where aqueous protons are utilized selectively for CO_2 reduction rather than hydrogen generation. Our strategy for CO_2 reduction involves the design of new homogeneous catalysts with tunable geometries and polyaromatic frameworks with increased delocalization to lower overpotentials for catalysis. We report a family of biaryl-bridged pyridyl-*N*-heterocyclic carbene-based ligands and their corresponding nickel complexes. Ligand synthesis, structural characterization of complexes, and their application in electrocatalytic CO_2 reduction are discussed.

DEDICATION

This thesis is dedicated to my friends and family who have supported me and guided me through all of my endeavors. They have given their time to listen to countless discussions they did not understand. They have been my rock and support through times of triumph and failure. I thank you, because you are truly the ones who have helped me to reach this goal.

In particular, this thesis is dedicated to Mrs. Meisha Sparks, my first chemistry teacher. She taught me a love for chemistry that has never left me. I cannot thank you enough for how you have helped to shape my life and my future.

LIST OF ABBREVIATIONS AND SYMBOLS

Btu	British Thermal Unit
EIA	U.S. Energy Information Administration
kg	Kilogram
kWh	Kilowatt hour
CO_2e	Carbon dioxide emission
CO_2	Carbon dioxide
CH_4	Methane
N_2O	Nitrous oxide
ppb	Parts per billion
ppm	Parts per million
ATP	Adenosine triphosphate
$NADP^+$	Nicotinamide adenine dinucleotide phosphate
NADPH	Reduced nicotinamide adenine dinucleotide phosphate
C	Chromophore

D	Donor
Cat_{Ox}	Oxidative Catalyst
Cat_{Red}	Reductive Catalyst
H_2O	Water
PEM	Proton Exchange Membrane
hν	Light
e^-	Electron
H^+	Proton
PMD	Photochemical Molecular Device
HCO_2H	Formic Acid
CH_3OH	Methanol
PCET	Proton Coupled Electron Transfer
V	Volts
Ni	Nickel
Cyclam	1,4,8,11-tetraazacyclotetradecane
KCl	Potassium chloride

GC electrode	Glassy carbon electrode
Dimethylcyclam	1,8-Dimethyl-1,4,8,11-tetraazacyclotetradecane
Tetramethylcylam	1,4,8,11-Tetramethyl-1,4,8,11-tetraazacyclotetradecane
DMC	Dimethylcyclam
TMC	Tetramethylcyclam
$TBAPF_6$	Tetrabutylammonium hexafluorophosphate
mV	Millivolts
s	Seconds
CV	Cyclic voltammogram
CPE	Controlled potential electrolysis
mA	Milliamps
cm	Centimeters
mM	Millimolar
hr	Hour
DFT	Density Functional Theory
kJ	Kilojoules

mol	Mole
M	Molar
SCE	Saturated calomel electrode
TOF	Turn over frequency
mL	Milliliter
°C	Degrees Celsius
g	Gram
mmol	Milimole
TLC	Thin-layer chromatography
NMR	Nuclear magnetic resonance
DME	Dimethoxyethane
MeCN	Acetonitrile
µA	Microamps
Fc	Ferrocene
TFE	Trifluoroethanol
MeOH	Methanol

i_p	Difference between current and background, inert atmosphere
i_{cat}	Difference between current and background, catalytic atmosphere

ACKNOWLEDGMENTS

I would like to thank my research advisor, Dr. Jonah Jurss for providing an opportunity to learn and pursue a project that I was very passionate about. I would also like to thank my committee members, Dr. Jared Delcamp and Dr. Jason Ritchie, for their support along the way.

I would like to give special thanks to Dr. Jared Delcamp and his group for providing me a collaborative opportunity and my first publication.

In addition, I would like to give special recognition to wonderful undergraduate researchers, Logan B. Bell, Jacqueline P. Gledhill, and Ryan A. Higgins, without whom this thesis would not have been possible.

Lastly, I would like to thank my fellow graduate research students who have provided me with plenty of good memories and support over the past two years. You have been my source of new knowledge and immense encouragement. This thesis could not have been completed without you.

TABLE OF CONTENTS

LIST OF TABLES

LIST OF FIGURES

INTRODUCTION

The need for new forms of energy

It was reported in 2014 that the energy consumption of the United States was 98.505 quadrillion Btu of energy.[1] Of this energy, 82% was derived from fossil fuels, consisting of coal, oil, and natural gas.[1] The EIA has projected a 48% increase in energy consumption of the world between the years of 2012 and 2040.[2] This increase in energy consumption is to be expected due to increased mobilization, decrease in underdeveloped nations, and as the world population continues to increase. The population is projected to increase from the 7.3 billion people that were reported in 2014 to over 9.7 billion by 2050.[3]

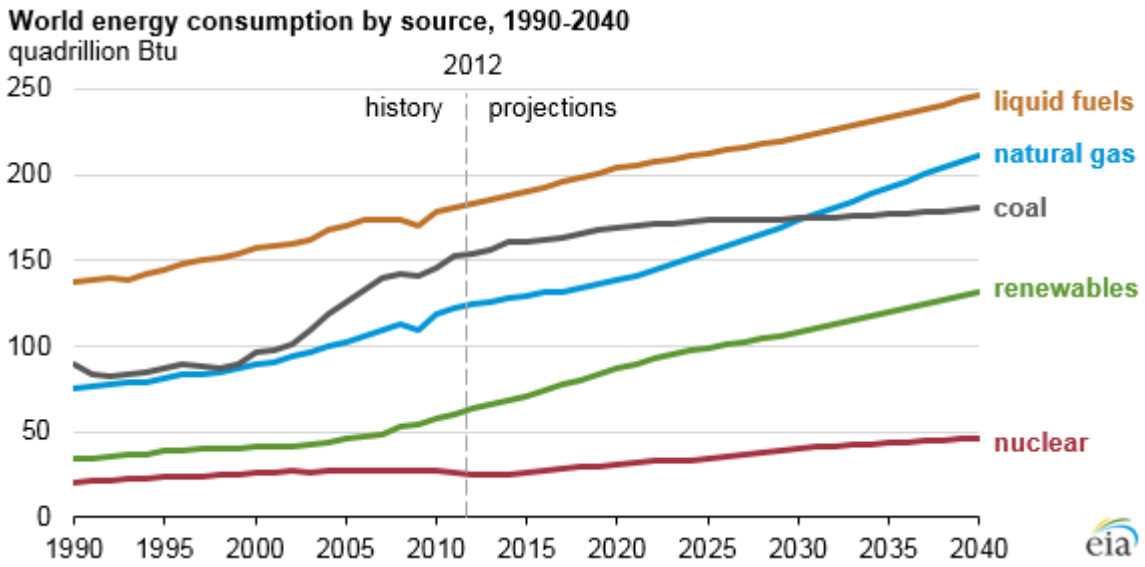

Figure 1: Chart showing the history of energy consumption by source and projections for future consumptions. A stark rise in renewable energy is predicted by this chart over what is presently being used or available. It will be the role of scientists to find viable and affordable alternatives to make this a reality.[2]

There are issues associated with the combustion of fossil fuels. The 82% of energy that comes from fossil fuels is made up of 22% coal, 34% natural gas, and 44% oil.[1] As depicted in Figure 2, these energy sources produce the majority of the carbon dioxide emissions when consumed. Carbon dioxide, commonly known as a greenhouse gas, absorbs heat that would be otherwise emitted into space. With the current dependence on fuel sources, there is no surprise that the planet is experiencing various forms of climate change.

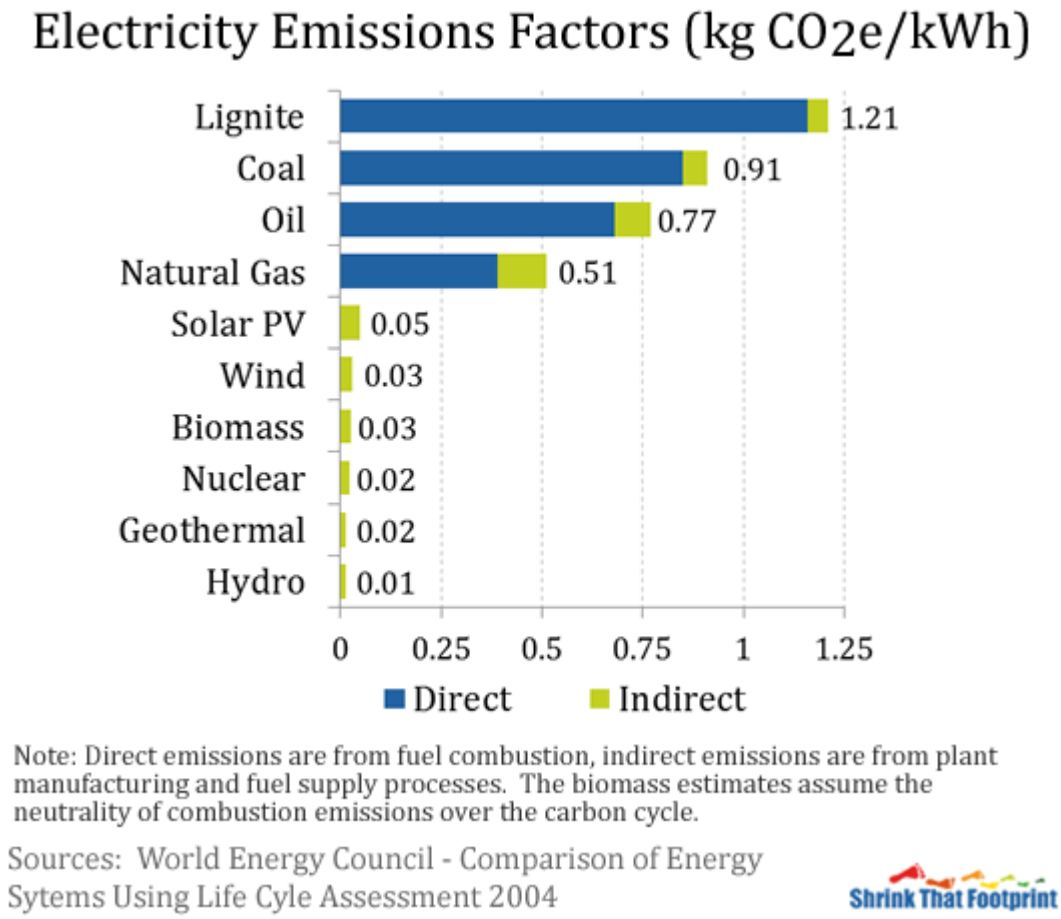

Figure 2: Graph showing the amount of carbon dioxide that is produced by the consumption of each of these sources of energy. It should be noted that fossil fuels, which currently dominate energy consumption at 86%, offer the largest production of carbon dioxide by far.[32,33]

Greenhouse emissions from combustible fuel sources are becoming more concentrated over the past 2000 years. In Figure 3, a spike in carbon dioxide emissions can be observed around the early 1800's due to the beginning of the Industrial Revolution. Scientists currently predict that the atmospheric concentration of carbon dioxide has a critical limit of 450 to 500 parts per billion (ppb). After this limit is reached, catastrophic side effects will ensue.[6-9] Theoretically, Figure 3 portrays an exponential increase surpassing the critical limit of carbon dioxide if no change is found soon.

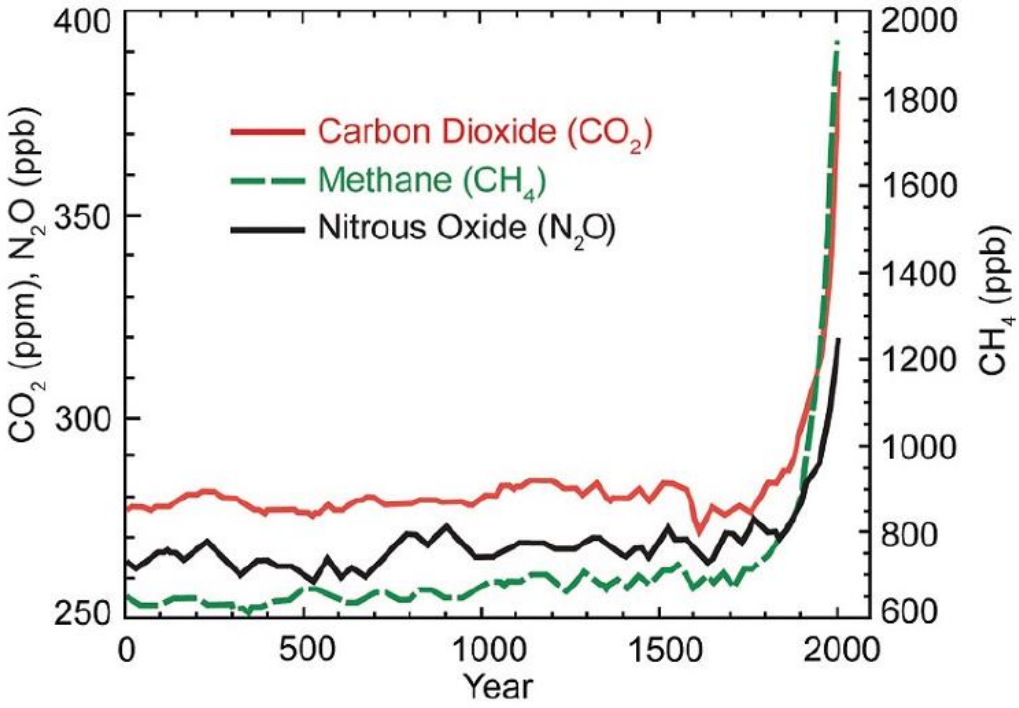

Figure 3: Graph depicting the atmospheric concentrations of some common greenhouse gases. It would appear from the graph that methane is as critical if not more so than carbon dioxide. It

should be noted, however, that the methane and nitrous oxide concentrations are given in parts per billion (ppb) while carbon dioxide is listed in parts per million (ppm).[4,5]

Knowing the limited supply in current resources, the scientific community has invested significant time and effort toward addressing the energy crisis. Energy initiatives primarily focus on photochemical molecular devices. These devices feature a catalytic center that can be utilized for water oxidation or carbon dioxide reduction. Currently, my research focuses on these catalytic centers as well as the potential to improve the stability and cost-effectiveness for photochemical devices.

Artificial photosynthesis

In nature, scientists focus their inspiration on photosynthesis as a means to storing solar energy in the chemical bonds of fuels and reducing the amount of carbon dioxide in the atmosphere. Photosynthesis is a chemical process found in plants and the major contributor in carbon dioxide reduction. Upon cellular uptake, carbon dioxide is converted into carbohydrates using water as the reducing agent and diatomic oxygen. Vegetation alone, can reduce 5.8 billion tons of carbon dioxide yearly.[10] A conceptual process of photosynthesis is shown in Figure 4.[11] Photosystem II acts as an oxidative catalyst to participate in water oxidation, therefore supplying the cell with electrons and free protons to create precursors later in this process. The free protons create an electrochemical gradient inside the cell that is used to drive ATP synthase. This ability overcomes the required activation energy to turn ADP into ATP to be used in the Calvin cycle.[14] The protons are also used to reduce $NADP^+$ to NADPH to be used in the Calvin cycle. The electron transport chain in photosynthesis is often referred to as the "Z scheme" due to the shape of the electron pathway with respect to energy.[13] The process works by utilizing a photon to

excite an electron.[12] The electron is in the ground state of photosystem 2. This electron is then excited by a photon of light into the excited state. The electron moves down a certain pathway that is lower in energy until arriving in the ground state of Photosystem I. The electron absorbs another photon and is sent back into the excited state, subsequently performing the reduction to NADPH.[12]

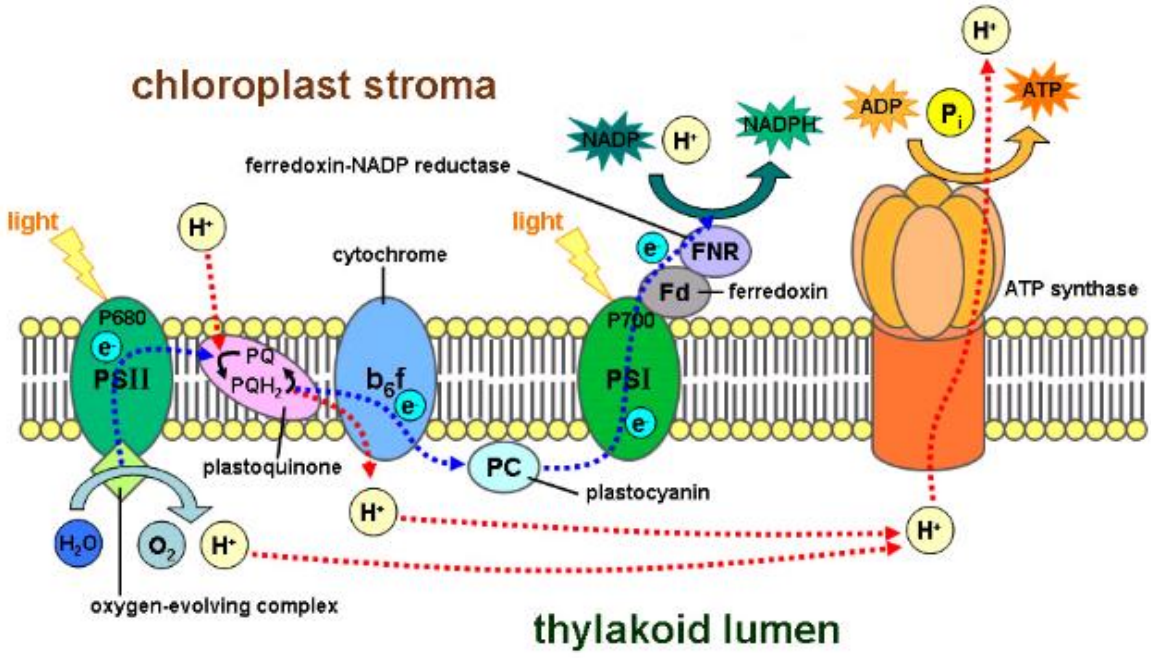

Figure 4: Picture depicting photosynthesis as performed by plants. Photosystem II performs water oxidation to create free protons which can be used in various ways throughout the photosynthetic process.[17]

Scientists are wanting to replicate the photosynthesis process observed in plants through the help of photochemical devices. Artificial photosynthesis can be achieved through two half-reactions, one at the anode and one at the cathode of a photochemical device as shown in Figure 5. Reductive and oxidative half-cells can be developed and optimized separately, but must be

combined as shown in Figure 5 to achieve artificial photosynthesis. This research specifically focuses on the reductive catalyst circled in red.

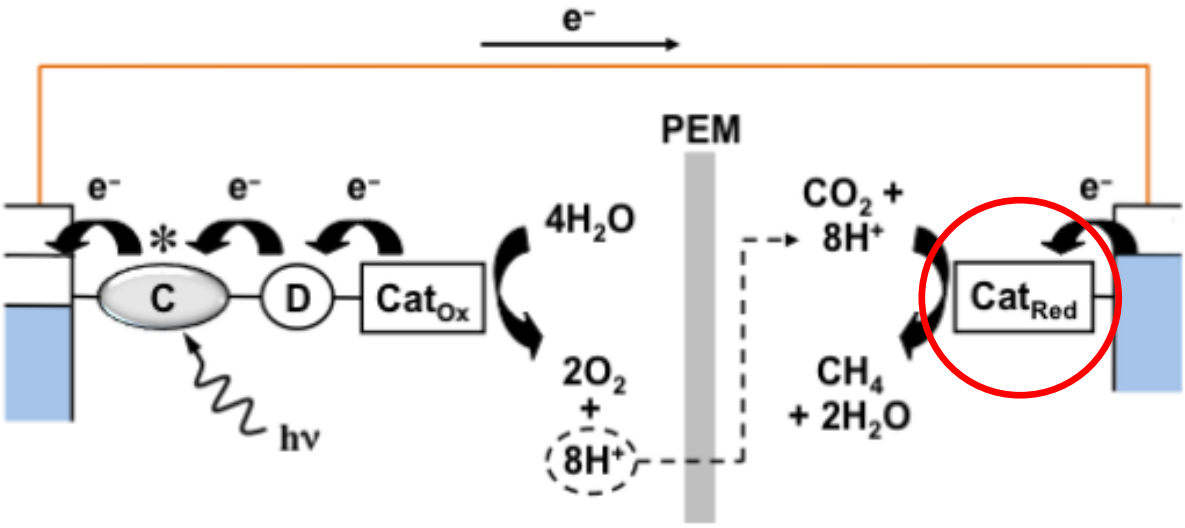

Figure 5: Photosynthesis as performed by two half cells combined to perform oxidative and reductive chemistry. The reductive catalyst, circled in red, is the focal point of this research.[15]

A proton exchange membrane (PEM) is also an important component of this photochemical molecular device. PEMs allow the transfer of free protons created from water oxidation down a gradient to the cathode for reductive chemistry.[17] The membrane is essential for the separation of the oxygen from the cathode. If not kept in check, the oxygen can be reduced at the cathode rather than the desired substrate and potentially explosive mixtures of hydrogen and oxygen can be produced. Proper separation is required to avoid this dangerous outcome.

Thermodynamics and value of carbon dioxide reduction

The process of these common energy reductions can be explained with thermodynamics. Carbon dioxide is a difficult molecule to activate due to its linearity and nonpolar characteristics. Currently, the focus of most research is reducing carbon dioxide into carbon monoxide. Table 2 indicates that it is easier to reduce carbon dioxide into methane from an applied potential standpoint. However, 8 electrons and 8 protons raises a kinetic issue. This requires a catalyst to bring carbon dioxide together with eight protons and eight electrons. Unfortunately, current catalysts to date cannot handle enough charge buildup to facilitate a process for this requirement of electrons.

Table 1 Electrochemical reduction of CO_2 in the presence of a proton source (aqueous solution, pH 7, *vs.* NHE)

Selected reduction reactions of CO_2	E^o/V
$CO_2 + e^- \rightarrow CO_2^{\bullet -}$	−1.90
$CO_2 + 2H^+ + 2e^- \rightarrow CO + H_2O$	−0.53
$CO_2 + 2H^+ + 2e^- \rightarrow HCO_2H$	−0.61
$CO_2 + 6H^+ + 6e^- \rightarrow CH_3OH + H_2O$	−0.38
$CO_2 + 8H^+ + 8e^- \rightarrow CH_4 + 2H_2O$	−0.24

Table 1: This table depicts the common thermodynamic potentials needed to reduce carbon dioxide to certain products. These values were taken in an aqueous solution at pH 7.[18,19]

Proton coupled electron transfer (PCET) is a key component for the reduction process. Table 1 establishes the thermodynamic potential required to reduce carbon dioxide. With a single electron, production of the radical species is formed. The radical form is more than three times more negative than the other potentials due to the instability of this species. PCET avoids the

radical intermediate and the possibility of charge build up.[19] These two factors allow the thermodynamics to be far less negative for the other potentials.

To perform these reductions effectively, catalysts must be incredibly selective. Thermodynamic potential for proton reduction occurs at -0.42 V at pH 7, making it more favorable than the alternative reduction of carbon dioxide into carbon monoxide. The reduction process requires 2 electrons and 2 protons, which makes this process kinetically favorable. An unselective catalyst would perform proton reduction first before any reductive chemistry could occur with carbon dioxide.

Figure 6 explains a potential application of carbon dioxide reduction; more specifically, the synthesis of other organic molecules. Currently, the carbon source for synthesizing these molecules is often petroleum, a resource that is becoming more difficult to obtain. Through carbon dioxide reduction, the reduced products could be utilized as a C1 feedstock instead of petroleum conversion.[23,38] Profit is also to be made using carbon dioxide reduction. Simple reduction to carbon monoxide, the polarity of this particular molecule is much easier to activate. This product is roughly $1300 per ton. Another common goal of artificial photosynthesis is the ability to reduce the carbon dioxide into methanol. Methanol is valued at roughly $400 per ton. Last but not least, the reduction cycle could produce fuels that can be repeatedly used for combustion. This closed cycle will offer a viable fuel source for the future without further pollution of the atmosphere.

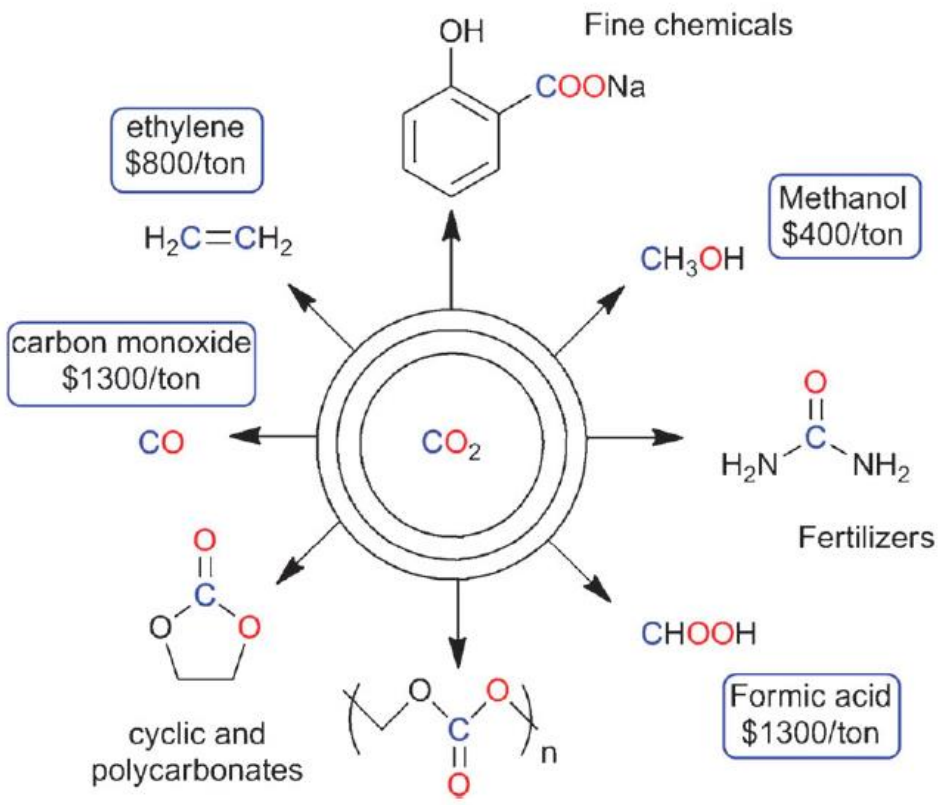

Figure 6: Common products that can be formed by utilizing carbon dioxide reduction.[18,20]

The value of the potential products is only part of the benefit in the attempts of carbon dioxide reduction. Current research has investigated the harmful effects to the environment. With these current issues, the proposed solution is to synthetically produce catalysts that mimic the reductive chemistry in plants as well as maintaining a sense of cost effectiveness and retaining selectivity. The cost effectiveness of these catalysts would become better if earth abundant metals such as nickel are utilized.

NICKEL CATALYSTS

Nickel Cyclam

Molecular nickel catalysts for carbon dioxide reduction begins with [Ni(1,4,8,11-tetraazacyclotetrdecane)]$^{2+}$- [Ni(cyclam)]$^{2+}$. This catalyst has been extensively studied as a model catalyst for carbon dioxide reduction.[28] This catalyst features relative stability and selectivity for the reduction of carbon dioxide.

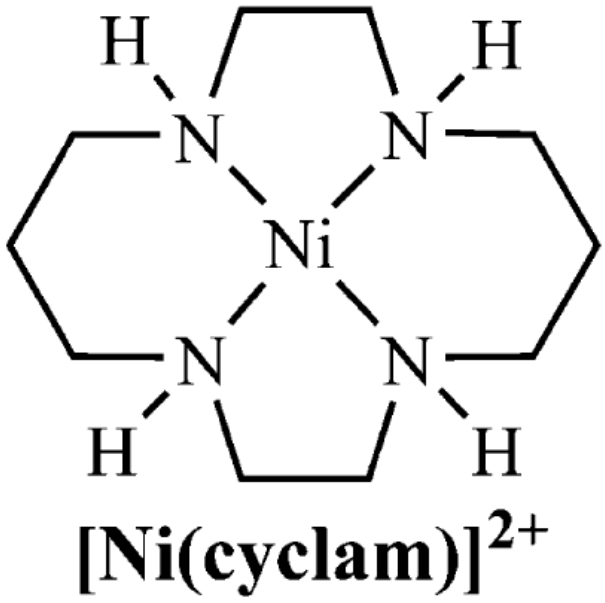

Figure 7: The above show the molecular structure for [Ni(1,4,8,11-tetraazacyclotetradecane)]$^{2+}$ which is more commonly referred to as [Ni(cyclam)]$^{2+}$. [24]

$[Ni(cyclam)]^{2+}$ is unique due to its ability to effectively reduce carbon dioxide to carbon monoxide. This process could even be done within an aqueous environment. As discussed earlier, the thermodynamic potential for proton reduction is more favorable than the reduction of carbon dioxide. Earlier studies with $[Ni(cyclam)]^{2+}$ were conducted using a mercury electrode. This type of electrode has a very negative potential for proton reduction, making it difficult to determine if $[Ni(cyclam)]^{2+}$ was selective or the negative potential aided in the perceived selectivity.[26] $[Ni(cyclam)]^{2+}$ also adsorbs to the mercury electrode, which increases the catalytic activity.[24] The Kubiak group investigated the catalyst using a glassy carbon electrode. In doing this, the electrode offered less aid to the catalyst and has become more popular in recent literature.

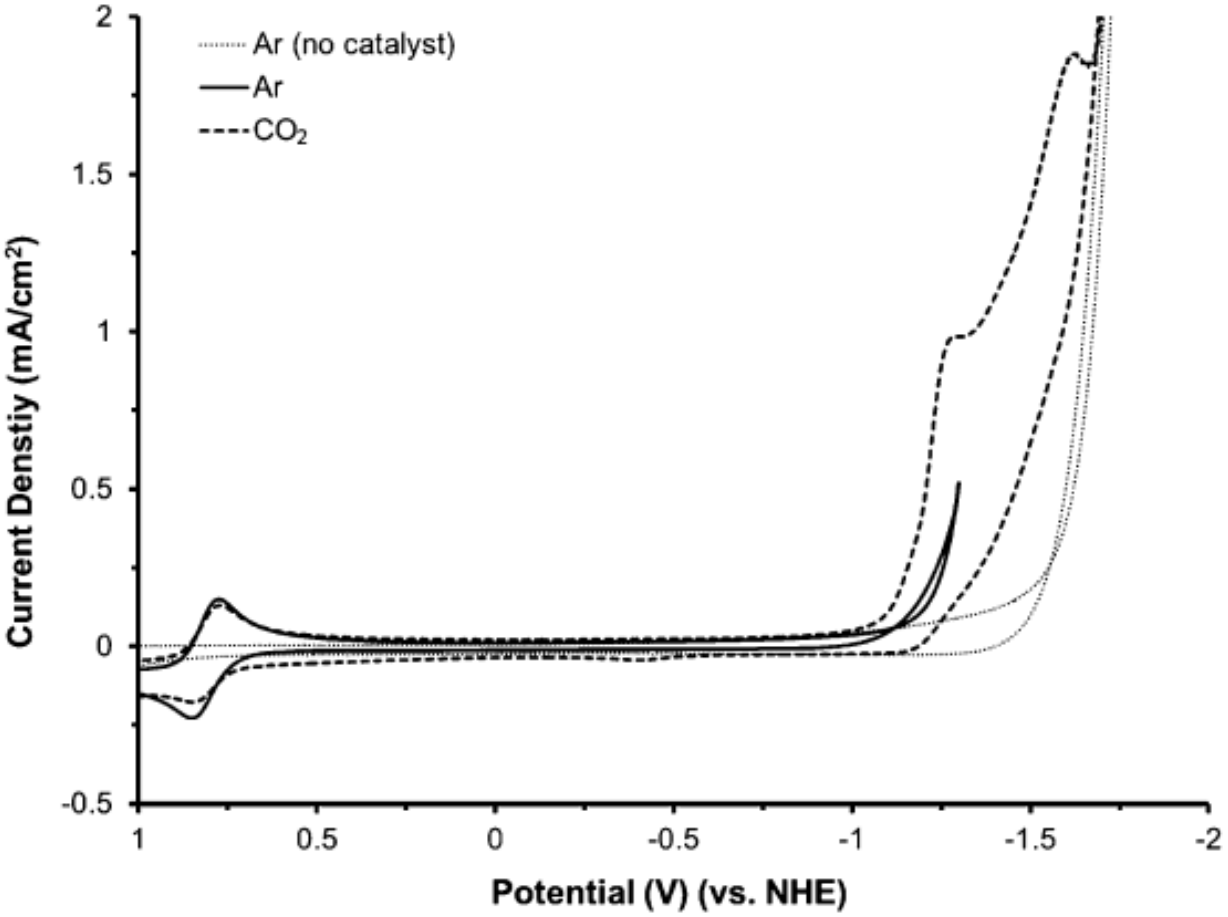

Figure 8: Cyclic voltammograms of 1 mM Ni(cyclam)$^{2+}$ in aqueous 0.1 M KCl, GC electrode; scan rate = 100 mV/s.[24]

Figure 8 is a study by the Kubiak group with [Ni(cyclam)]$^{2+}$ exposed to a carbon dioxide environment. The changes of the aqueous solution allow the potential window of the solvent for the glassy carbon electrode. Limiting the solvent window makes it impossible to observe the second reduction of the nickel center. The Kubiak group mentioned that this area is dominated by proton reduction at the glassy carbon electrode. The limited solvent window makes it impossible to observe the second reduction potential of the nickel center. The Kubiak group also reported that under a catalytic carbon dioxide environment and a potential held at -1.3 V, the catalyst displayed a Faradaic efficiency of 90% for carbon monoxide with no hydrogen gas

detected.[24] Given a more negative potential at -1.6 V, the Faradaic efficiency of 90% for carbon monoxide with a 20% Faradaic efficiency for hydrogen gas.[24] This implies that the catalyst is selective for carbon dioxide and retains this selectivity even at very negative potentials.

Methylation of Nickel Cyclam

The Kubiak group investigated the role of hydrogen atoms in the R positions and how they affect the reduction of carbon dioxide. Performing this investigation, the group synthesized a series of catalysts with methylation at different points. $[Ni(cyclam)]^{2+}$, $[Ni(dimethylcyclam)]^{2+}$ - [Ni(DMC)], and $[Ni(tetramethylcyclam)]^{2+}$ - [Ni(TMC)]. The various methylations led to more steric hindrance and a decreased possibility for participation in hydrogen bonding.

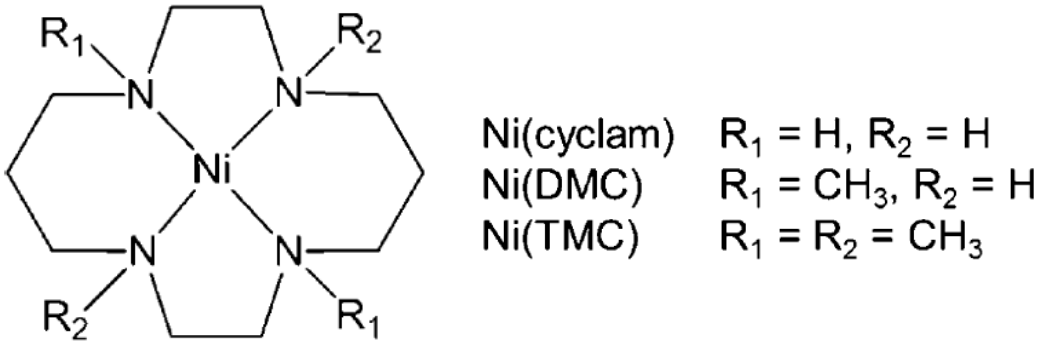

Figure 9: Structures of Ni(cyclam), Ni(DMC) (DMC = 1,8-Dimethyl-1,4,8,11-tetraazacyclotetradecane), and Ni(TMC) (TMC = 1,4,8,11-Tetramethyl-1,4,8,11-tetraazacyclotetradecane).[24]

Cyclic voltammetry was conducted to investigate the reactivity of these complexes. Ni(cyclam) was observed as the largest increase in current when placed under a catalytic atmosphere of carbon dioxide. This first reduction can be seen to occur at a more positive potential as the catalyst is methylated further.[33,34] Also note that an aqueous environment provides a proton source allowing the reduction process to begin at the first reduction of nickel. As previously stated, the reduction of carbon dioxide is a two electron process, therefore this does not generally occur until the second reduction of the metal center has occurred. Ni(DMC) has some catalytic activity after the second reduction of the nickel center, however, Ni(TMC) does not show the second reduction and little catalytic activity is observed.

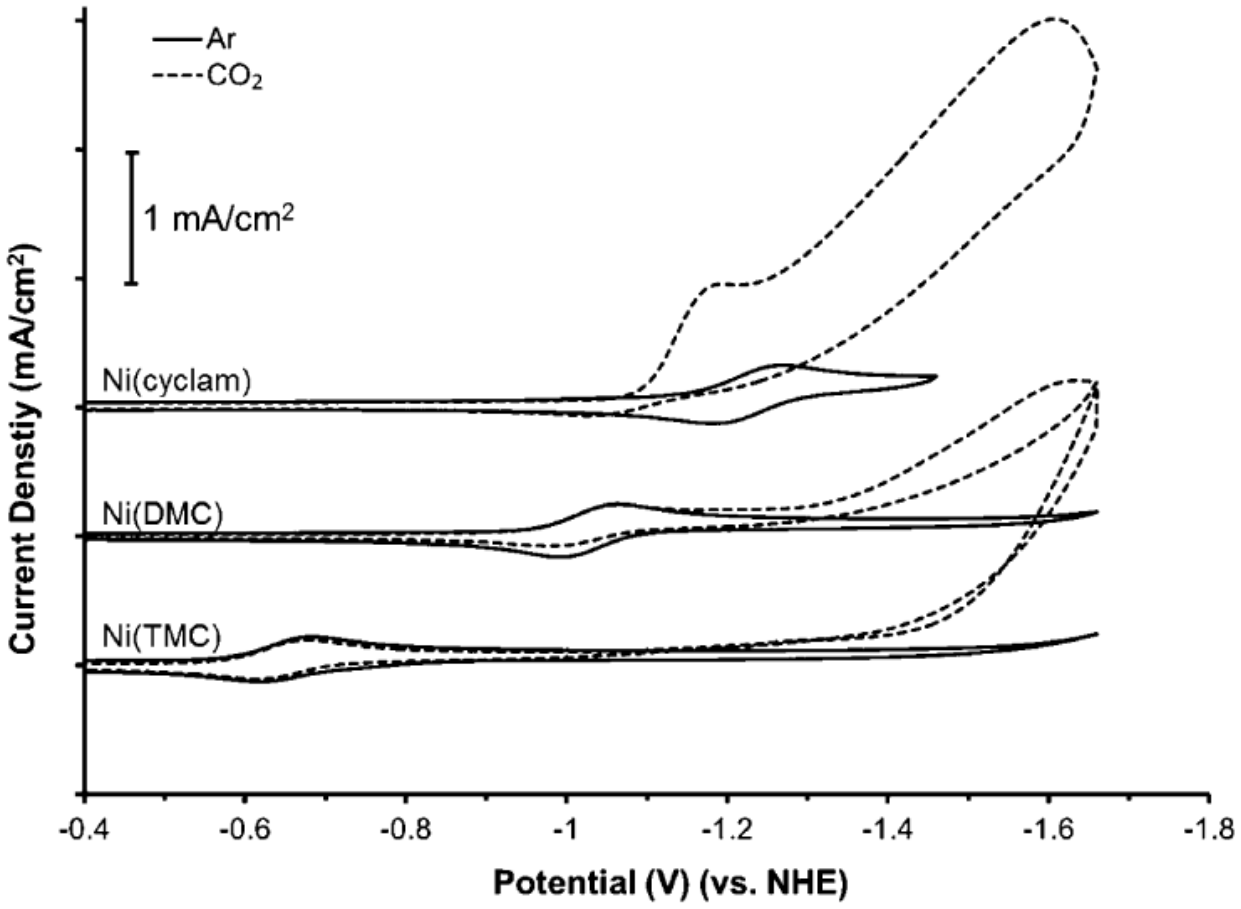

Figure 10: Cyclic voltamagrams of 1 mM Ni(cyclam)$^{2+}$, Ni(DMC)$^{2+}$, and Ni(TMC)$^{2+}$in a 0.08 M tetrabutylammonium hexafluorophosphate (TBA PF_6) solution as an electrolyte in 1:4 water/acetonitrile, GC electrode; scan rate = 100 mV/s.[24]

The potential of the catalytic peaks were taken from cyclic voltammograms (CV) of Ni(cyclam) and Ni(DMC). These potentials were also evaluated with controlled potential electrolysis (CPE). Results are reported in Table 2. Ni(cyclam) indicates selectivity at the first reduction potential and becomes less selective on the second potential. However, Ni(DMC) can only be studied on the second potential.[35] Ni(DMC) performs mostly proton reduction into Hydrogen gas. There is indication that methyl groups are involved with the binding of carbon dioxide to the catalyst, consequently hindering the catalyst's ability to reduce carbon dioxide.

Results of CPE in 1:4 Water/Acetonitrile[a]

		Faradaic efficiency (%)		
complex	potential (V)	CO	H_2	current density (mA/cm^2)
Ni(cyclam)	−1.21	90	0	1.8
Ni(cyclam)	−1.61	60	10	4.5
Ni(DMC)	−1.63	20	80	3.8

Table 2: 1 mM complex was held at the given potential for 1 hr, GC working electrode, 0.8 M tetrabutylammonium hexafluorophosphate electrolyte.[24]

Isomers of Nickel Cyclam

$[Ni(cyclam)]^{2+}$ has five possible isomers. Of these isomers, trans I and trans III are present in measurable amounts. Trans I is found 15% of the time while trans III is found 85% of the time.[36] These specific isomers can be found in Figure 11.

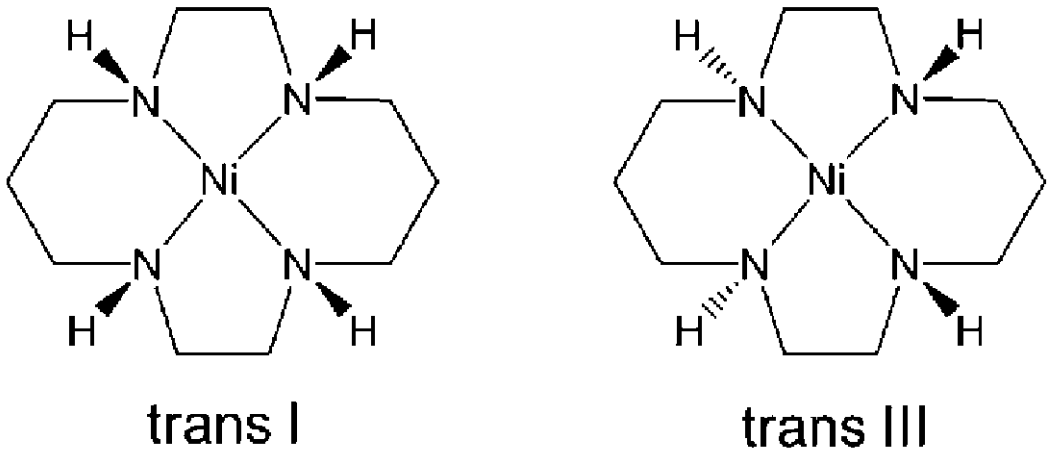

Figure 11: Structures of the Trans I and Trans III isomers of $[Ni(cyclam)]^{2+}$.[24]

The Kubiak group chose these isomers due to the availability in solution. DFT calculations were completed on the isomers in order to investigate the energy difference of binding. Results established that trans I isomer was more favorable with the binding of carbon dioxide by 21 kJ/mol.[24] With this being said, the theory behind this difference in energy is due to the oxygens on the carbon dioxide interaction with the protons of the two amines in trans I isomer. In trans III isomer, only one proton is available for interaction. The interaction scheme of trans I isomer is depicted in Figure 12.

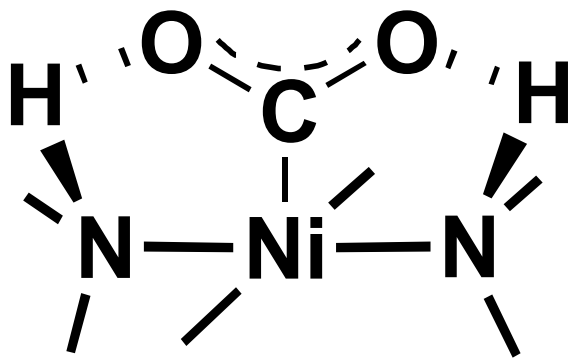

Figure 12: A proposed interaction of the two amine protons interacting with the carbon dioxide.

Kubiak noted that the activity of $[Ni(cyclam)]^{2+}$ is more reactive when a mercury electrode is used for studies.[25] A current assumption of this reactivity states that the adsorption of the $[Ni(cyclam)]^{2+}$ onto the surface of the mercury electrode could potentially force the catalyst into the favorable trans I isomer. The difference in the carbon dioxide binding energy with trans I isomer may yield to greater reactivity. Kubiak also made note of further investigating this concept to gain a better understanding.

Imidazole-pyridine based ligand for Nickel catalysts

The Chang Group proposed a new series of ligands that will be utilized with a nickel(II) center for carbon dioxide reduction. These new ligands feature a tetradentate framework involving a pair of imidazole and pyridine donors. Each ligand utilizes a different length of linking chains: methyl, ethyl, and propyl between the donor arms.[37] The differences were investigated through electrochemical studies. A general synthetic scheme for these complexes can be seen in Figure 13.

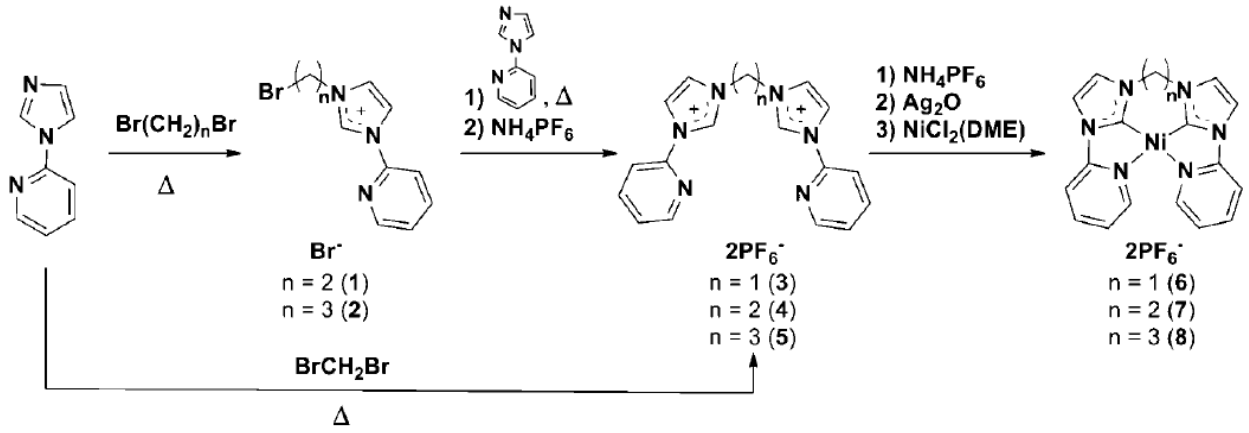

Figure 13: General synthetic pathway for series of imidazole-pyridine donor ligands and corresponding nickel catalysts.[37]

The oxidation states of nickel(II) and nickel(0) prefer the geometries of square planar and tetrahedral respectively. The Chang Group hypothesized that increasing the flexibility of the catalyst would aid in the geometric transitions previously mentioned when reduced.[37] This was studied through as systematic lengthening of the linking group between the two donor arms. Electrocatalytic experiments were completed with results show in Figure 14.

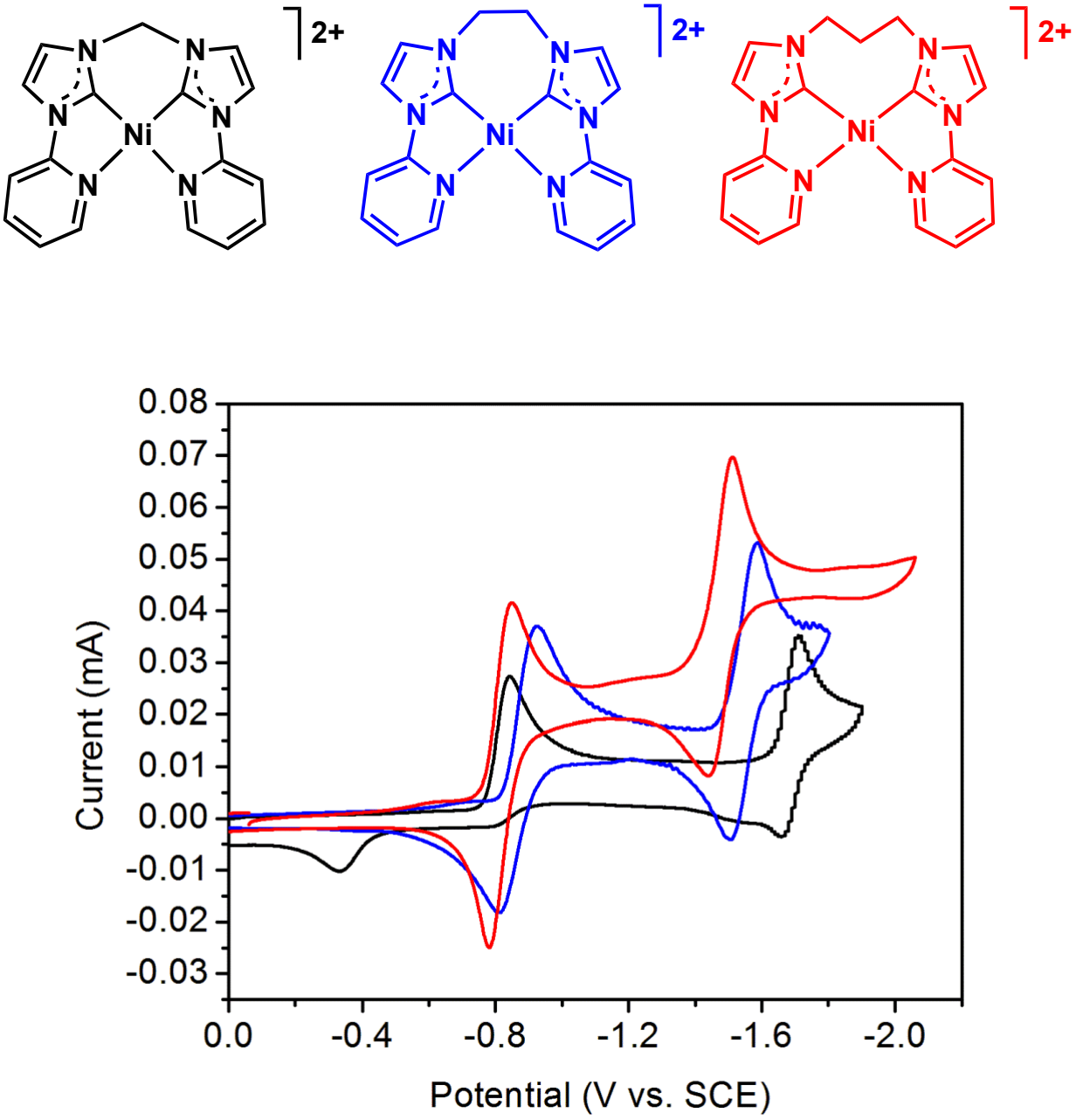

Figure 14: Cyclic voltammograms of 1 mM of the Chang complexes shown above. Glassy carbon disk electrode, 0.1 M $TBAPF_6$ in acetonitrile. A 200mV shift in the positive direction can be seen at the second reduction when comparing the methyl linker to the propyl linker. The complexes are color coated with the cyclic voltammagrams for ease of understanding.[37]

With the extension of the linking groups, there was an increase in the flexibility of the catalyst. These extensions also decreased the potential of the catalytic peak. The turnover frequency (TOF) also increases as the flexibility increased.[37] Both of these factors led the Chang Group to conclude that the flexibility of the catalyst has an effect on the overall catalytic activity. Proceeding forward, utilization of the propyl linker was the best option as a catalyst. This particular linker model will be used for different studies in carbon dioxide reduction.

Electron Delocalization and π Conjugation

The Chang Group focused their attention on the role of electron delocalization and the π conjugation of the imidazole-pyridine donors. A series of catalysts were synthesized to investigate these specific properties. Catalysts were modified using benzimidazole and isoquinoline bonded in different locations, as well as incorporating a benzimidazole catalyst with interrupted π conjugation.[39] General structures of these complexes are shown in Figure 15. These specific changes of the ligand were completed to study the effect on catalytic activity. There was indication that increasing the delocalization of the electrons within the ligand would possibly lead to increasing metal to ligand backbonding. The overall effect would make the nickel center more electron deficient and easier to reduce, consequently offering a lower overpotential and an increase in the catalytic activity.

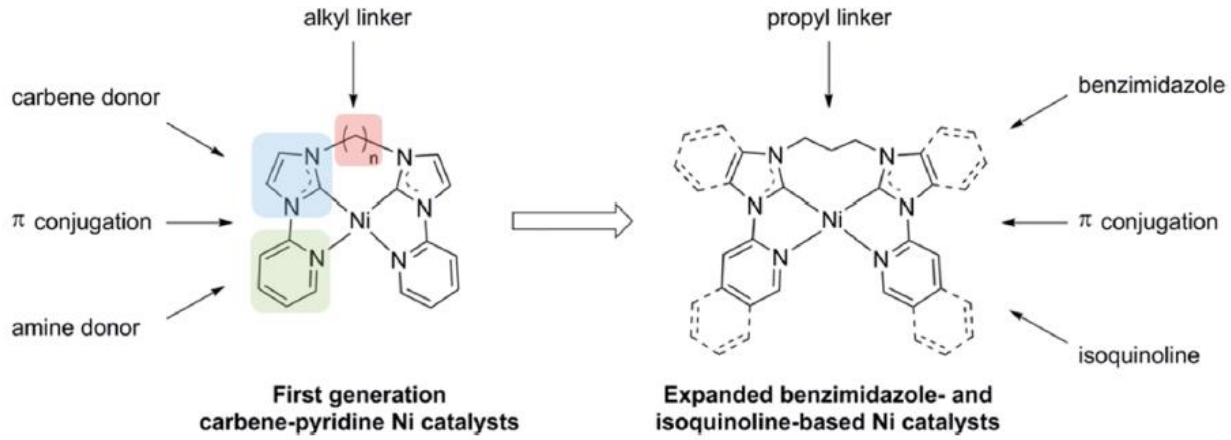

Figure 15: Basic framework for a new series of ligands that feature imidazole-pyridine donors with expanded aromaticity and delocalization.[39]

There was indication that isoquinoline groups have catalytic effects with the nickel center, similar to previous ligands without the added electron delocalization. Benzimidazole was found to have an extra reduction potential. This potential was observed to be more negative and the catalytically active reduction. Theoretically, this could be attributed to ligand-based reduction in the complex. The group synthesized a ligand to investigate the π conjugation between donors. A methyl group was added to the position denoted by the π conjugation in Figure 15. While maintaining the propyl linking group. This ensured the aromatic systems were fully unconjugated with each other. With further investigation, the Chang Group discovered that interrupting the π conjugation between the imidazole and pyridine groups located on the arms decreased catalytic activity almost entirely.[39] Crystal structures of these specific complexes are displayed in Figure 16.

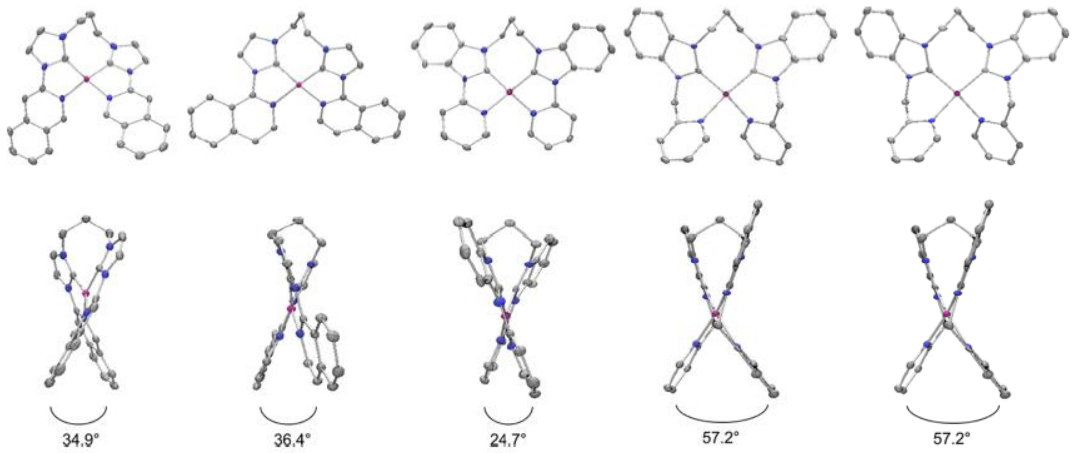

Figure 16: Crystal structures of new complexes derived to investigate the role of electron delocalization and π conjugation on catalytic activity.[39]

The observed moderate activity from nickel complexes and novel ligand framework is the inspiration for this thesis. Our ligands feature a biphenyl backbone to aid in a distorted tetrahedral framework. The proposed biphenyl backbone should increase the electron delocalization due to being fully conjugated.

SYNTHESIS

HD$_1$

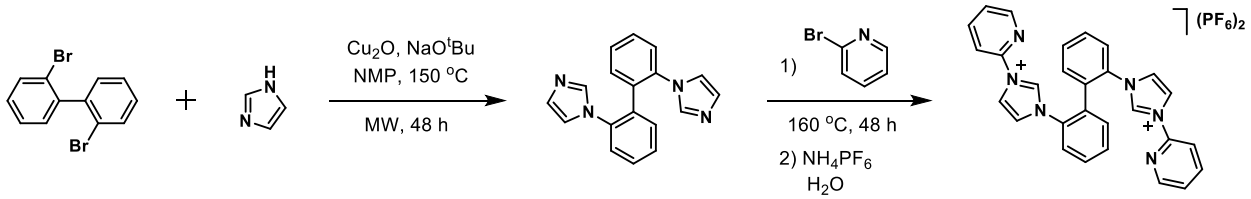

2,2'-di(1H-imidazol-1-yl)-1,1'-biphenyl

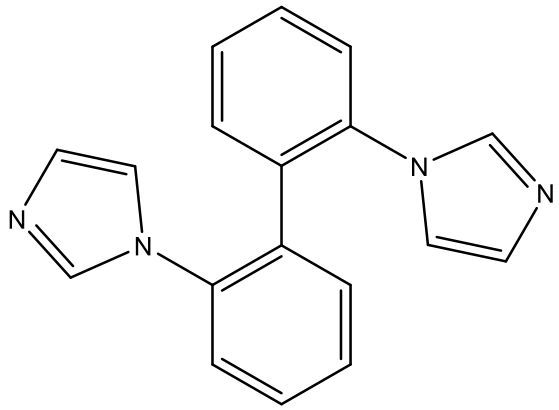

In a 30 mL microwave reaction flask, dibromobiphenyl (2.4960 g, 8 mmol), imidazole (2.1785 g, 32 mmol), copper (I) oxide (0.2289 g, 1.6 mmol), and sodium tert-butoxide (3.0752 g, 32 mmol) using n-methyl pyrrolidone (15 mL) as a solvent. The flask was placed in a Monowave 300 microwave synthesis reactor and set to run at 175 °C for four hour increments. The reaction

progress was monitored by TLC after each run. The reaction was shown to slow at 72 hours. The mixture was quenched with distilled water (200 mL) and added to a separatory funnel. The mixture was then extracted with diethyl either (4 x 100 mL). The organic phase was combined and rotovaped down to a 15 mL solution. This remaining solution was then purified utilizing a silica gel column eluting with 4:1 hexanes: ethyl acetate. Dibromobiphenyl came off the column first, followed by the product and then a monosubstituted version of the product.[49]

^{1}H NMR (500 MHz, Chloroform-*d*) δ 8.35 (s, 2H), 8.11 (d, *J* = 8.1 Hz, 3H), 8.02 (s, 0H), 7.63 (s, 2H), 7.52 (d, *J* = 8.2 Hz, 3H), 7.36 – 7.21 (m, 13H), 7.21 – 7.11 (m, 4H), 6.88 (s, 2H), 6.60 (s, 1H).

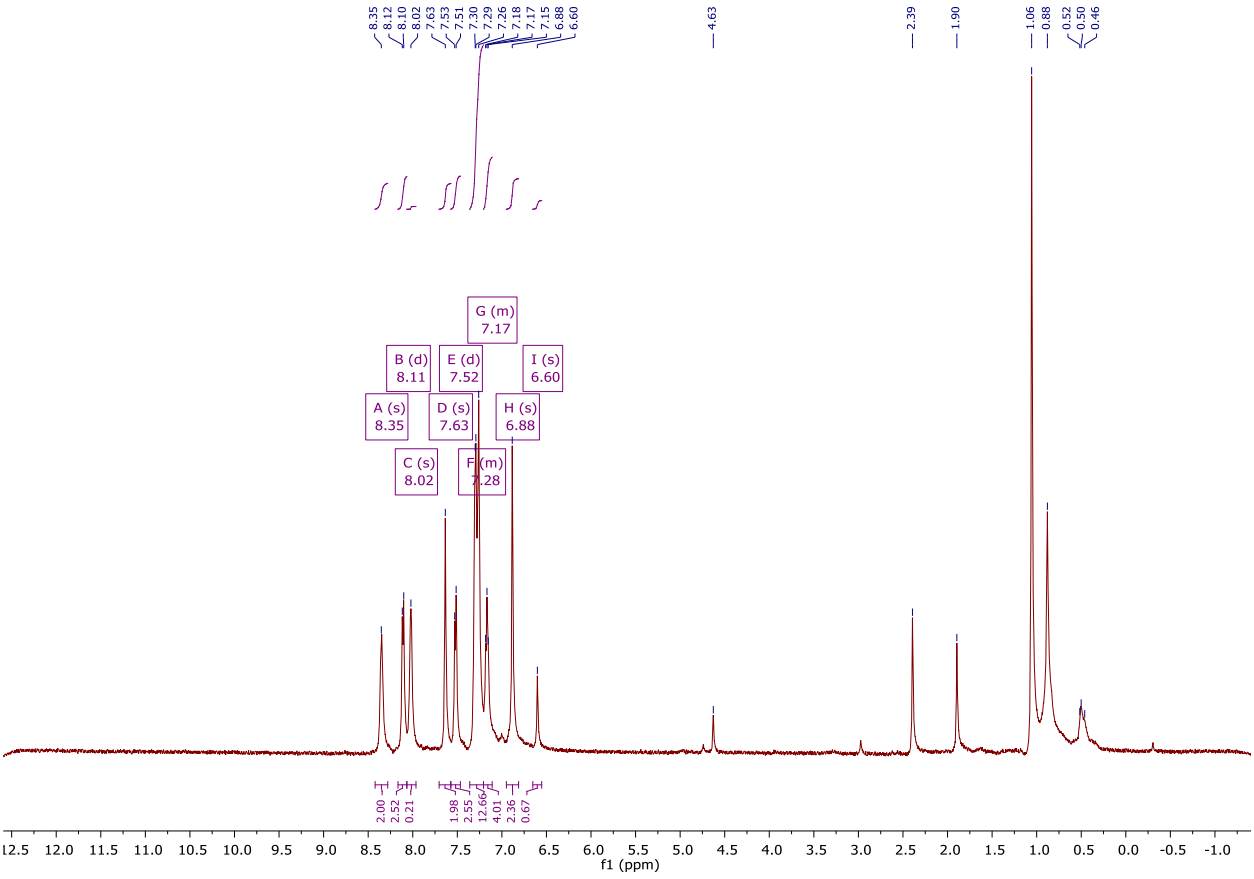

1,1'-([1,1'-biphenyl]-2,2'-diyl)bis(3-(pyridin-2-yl)-1H-imidazol-3-ium) hexafluorophosphate(V)

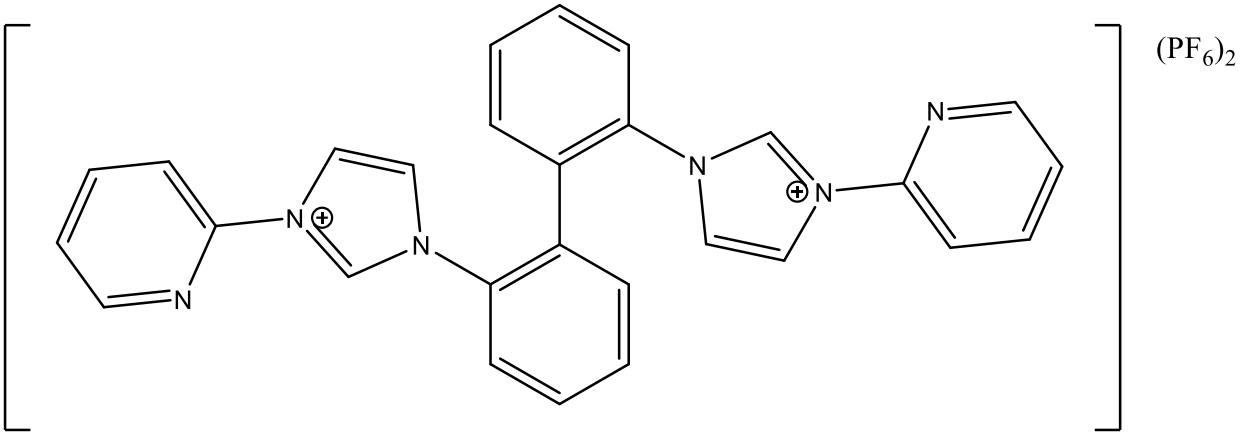

In a 25 mL pressure flask, 2,2'-di(1H-imidazol-1-yl)-1,1'-biphenyl (0.1000 g, 0.349 mmol) was dissolved in 5 equivalents of bromopyridine (0.17 mL, 1.745 mmol). The flask was placed in an oil bath at 160 °C for 48 hours. Upon completion, diethyl ether was added to the solution to precipitate the product. The product was then dissolved in acetonitrile (10 mL) ammonium hexafluorophosphate (0.1138 g, .698 mmol) was added. The solution was stirred under argon for 24 hours. The solution was centrifuged to remove the pellet and rotovapped down to yield product.[53]

[Ni(HD1)]$^{2+}$

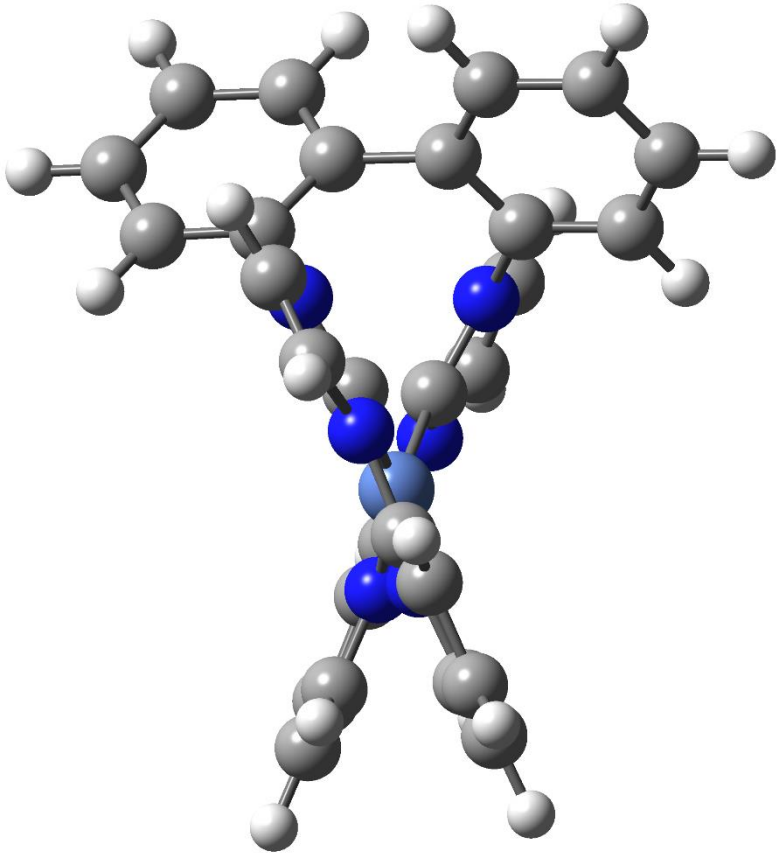

A DFT calculation for the proposed [Ni(HD1)]$(PF_6)_2$ is all that can be offered at this time due to difficulty in producing large enough quantities of pure ligand to pursue metalation. DFT shows a bite angle of the catalyst to be 32.5°.

HD2

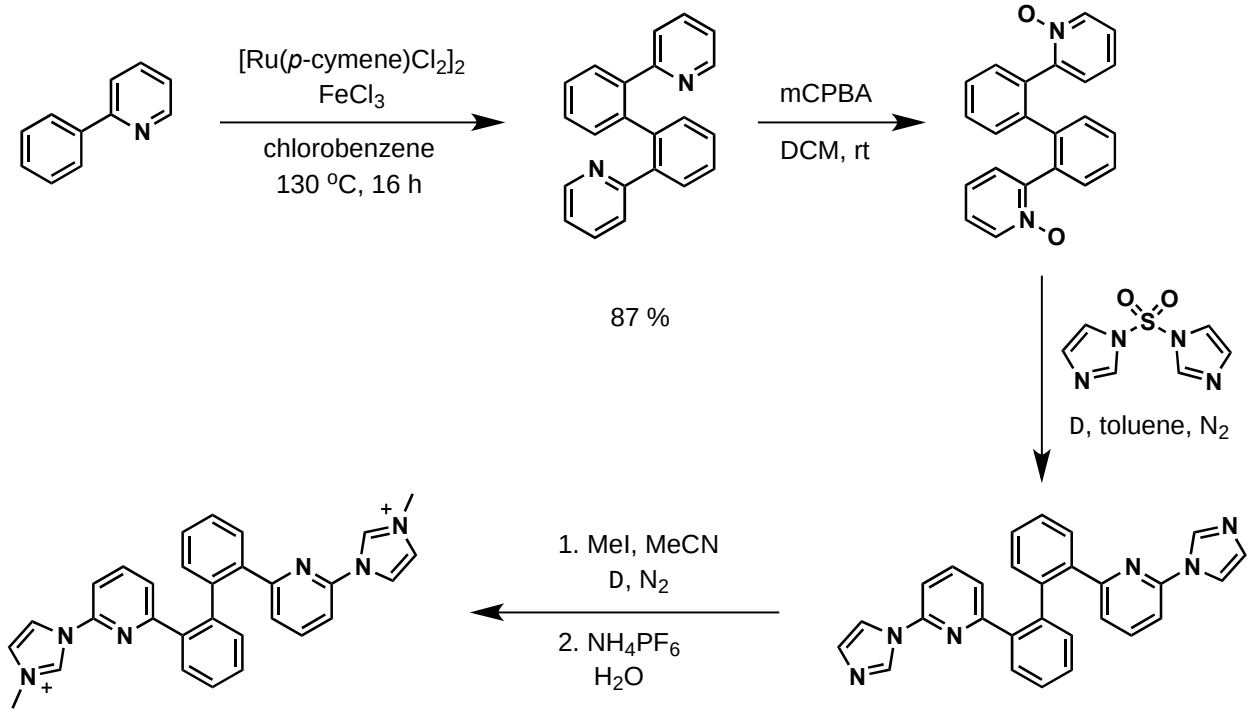

2,2'-di(pyridin-2-yl)-1,1'-biphenyl

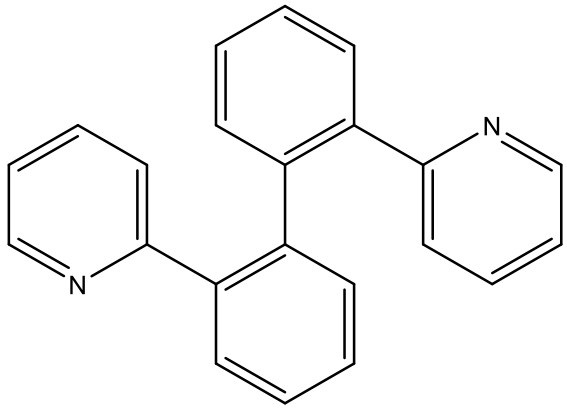

In a dry 350 mL pressure flask, combine $\{Ru(p\text{-cymene})Cl_2\}_2$ (0.3981 g, 0.65 mmol), 2-phenyl pyridine (3.72 mL, 26 mmol), and dry chlorobenzene (52 mL). Iron (III) chloride (3.3738 g, 20.8 mmol) was then added slowly. The pressure flask was flushed with nitrogen and closed. The reaction was heated at 130 °C for 2 days. Upon completion, the reaction was cooled to room temperature. Triethylamine (52 mL) and dichloromethane (52 mL) were then added and stirred overnight. The mixture was then run through a large silica gel plug with excess dichloromethane. For purification, a large column was run first with 1:1 diethyl ether: hexanes to remove impurities. The eluent was then switched to 1:1 ethyl acetate: hexanes to elute pure product.[50]

^{1}H NMR (500 MHz, Chloroform-*d*) δ 8.19 (d, *J* = 4.6 Hz, 2H), 7.40 (d, *J* = 7.8 Hz, 2H), 7.27 (q, *J* = 5.7, 4.9 Hz, 5H), 7.19 (t, *J* = 7.7 Hz, 2H), 7.12 (s, 1H), 6.92 – 6.81 (m, 1H), 6.64 (d, *J* = 7.9 Hz, 2H).

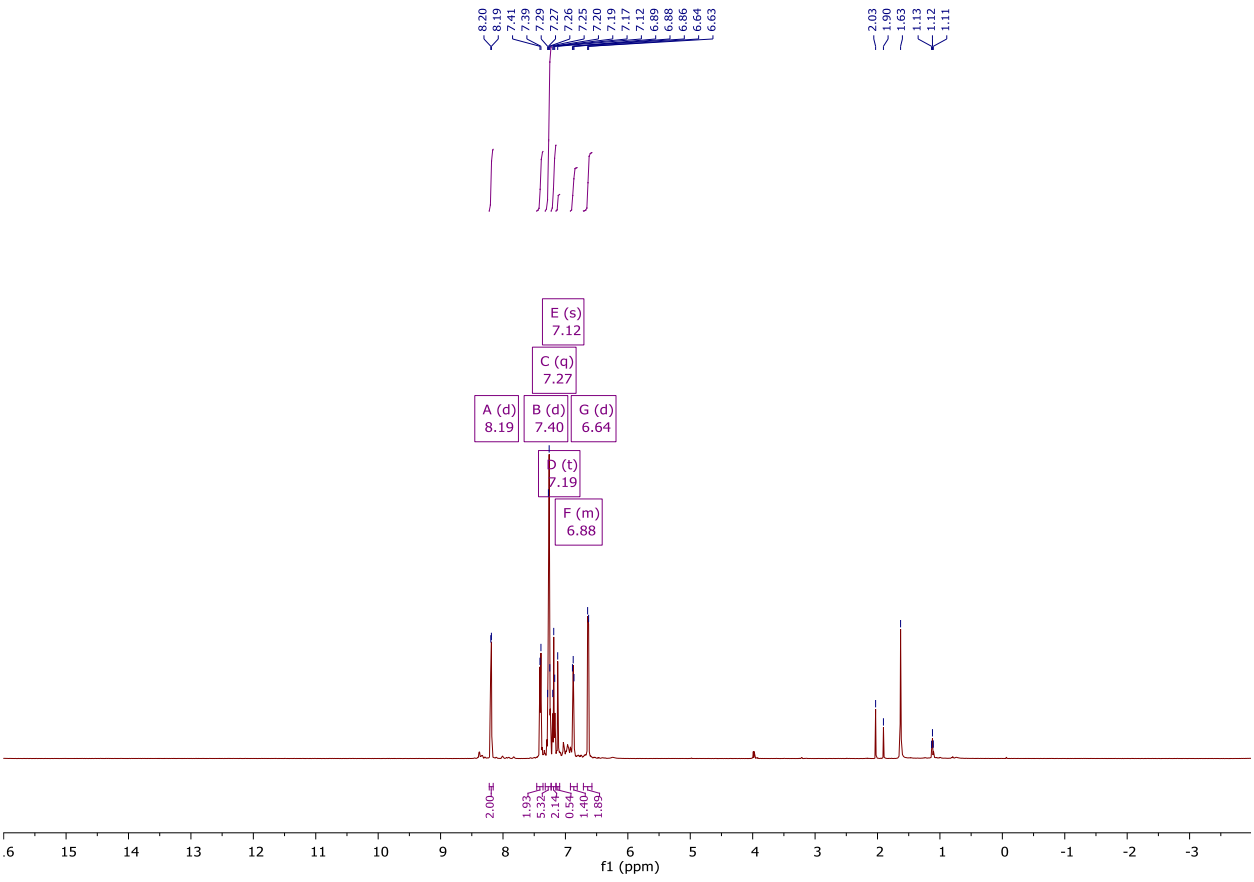

^{13}C NMR (126 MHz, $CDCl_3$) δ 158.16, 149.09, 139.98, 139.97, 135.32, 131.44, 130.15, 128.66, 127.85, 124.55, 121.31, 77.41, 77.16, 76.90.

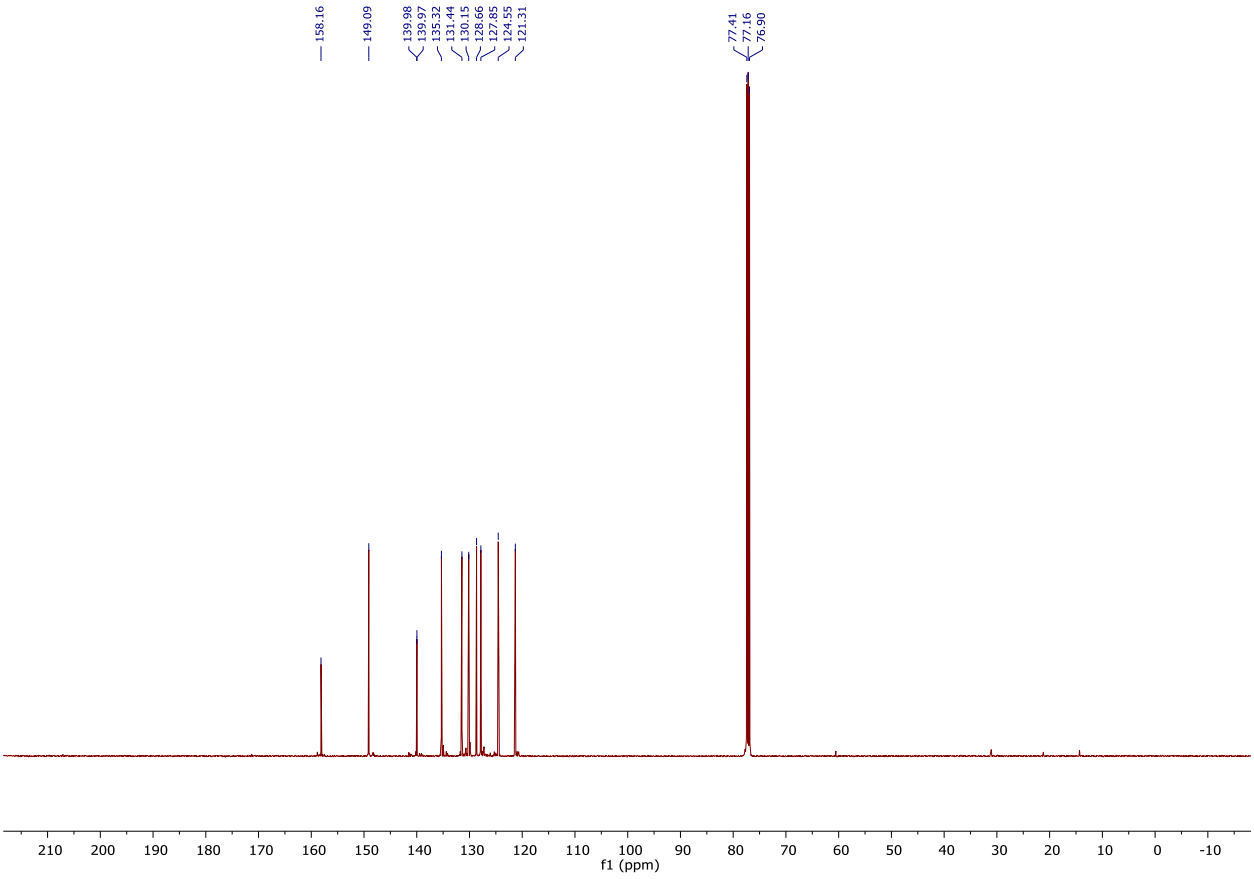

2,2'-([1,1'-biphenyl]-2,2'-diyl)bis(pyridine 1-oxide)

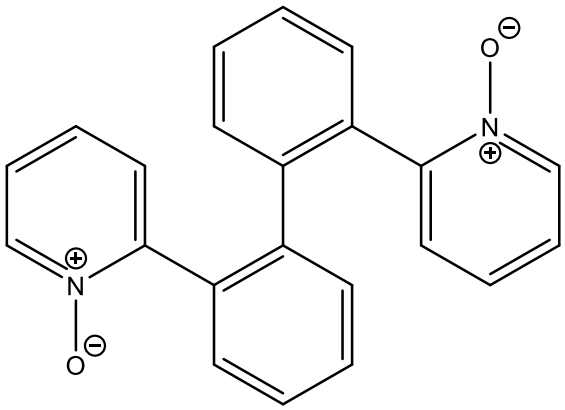

In a 100mL round bottom flask, 2,2'-di(pyridin-2-yl)-1,1'-biphenyl (0.5000 g, 1.621 mmol) was dissolved in chloroform (5 mL) and cooled to 0 °C. In a 20 mL screw cap vial, m-chloroperbenzoic acid (1.3990 g, 4.053 mmol) was dissolved in chloroform (15 mL) and cooled to 0 °C. This solution was added slowly to the 2,2'-di(pyridin-2-yl)-1,1'-biphenyl solution over 4 hours while remaining at 0 °C. After the addition was complete, the solution was stirred at room temperature for 2 days. The solution was rotovapped to near dryness and the product was precipitated using distilled water. The solid was then dissolved in chloroform and dried using sodium sulfate. The dried solution was concentrated and run on a silica gel plug with ethyl acetate to remove impurities. The pure product was then obtained by flushing the plug with methanol.[52]

^{1}H NMR (500 MHz, Chloroform-*d*) δ 8.18 (s, 0H), 7.62 (s, 0H), 7.47 (d, *J* = 7.0 Hz, 1H), 7.34 (t, *J* = 7.9 Hz, 2H), 7.26 (s, 2H), 7.18 (d, *J* = 5.9 Hz, 6H), 5.30 (s, 1H), 1.67 (s, 0H).

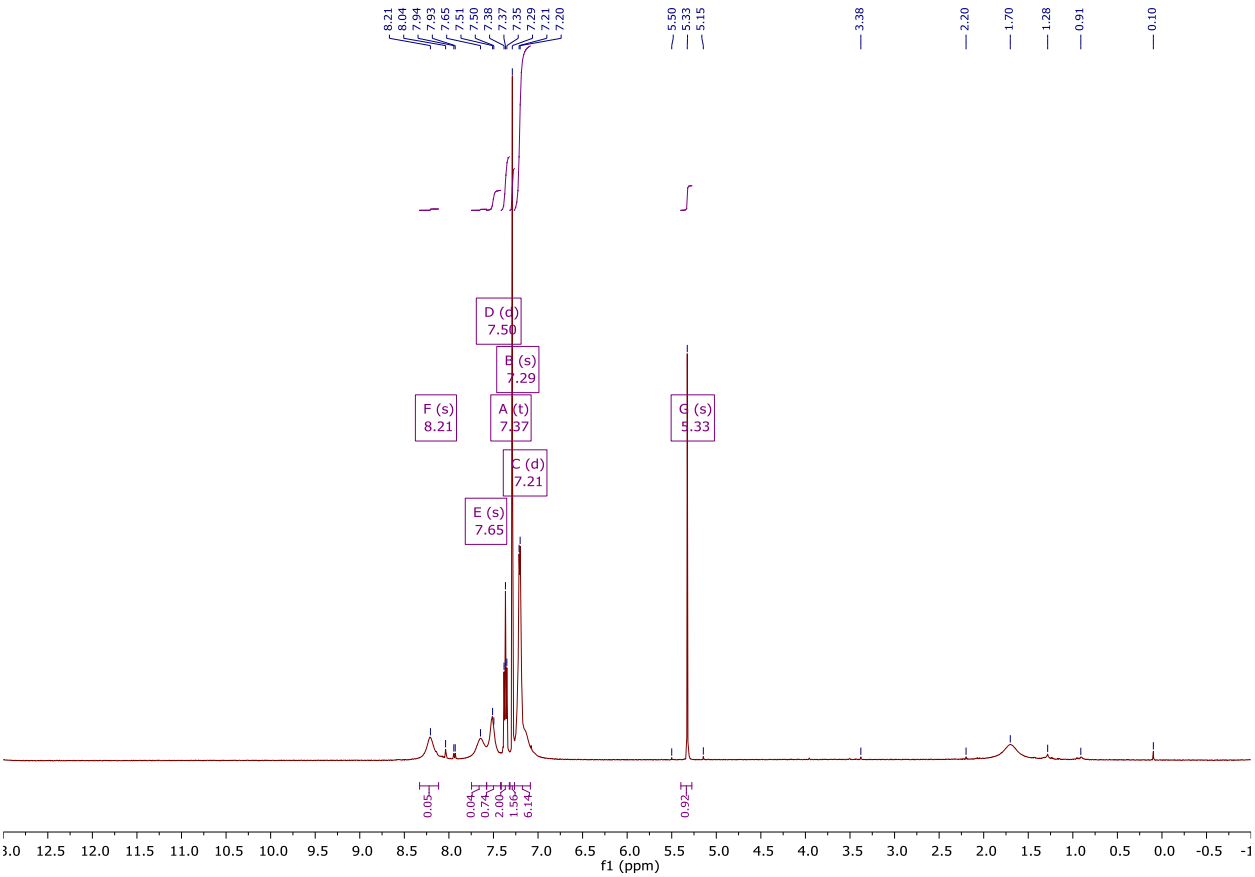

^{13}C NMR (126 MHz, $CDCl_3$) δ 150.13, 139.96, 139.79, 132.17, 130.81, 129.40, 128.96, 127.59, 125.61, 124.95, 77.41, 77.16, 76.91, 53.57.

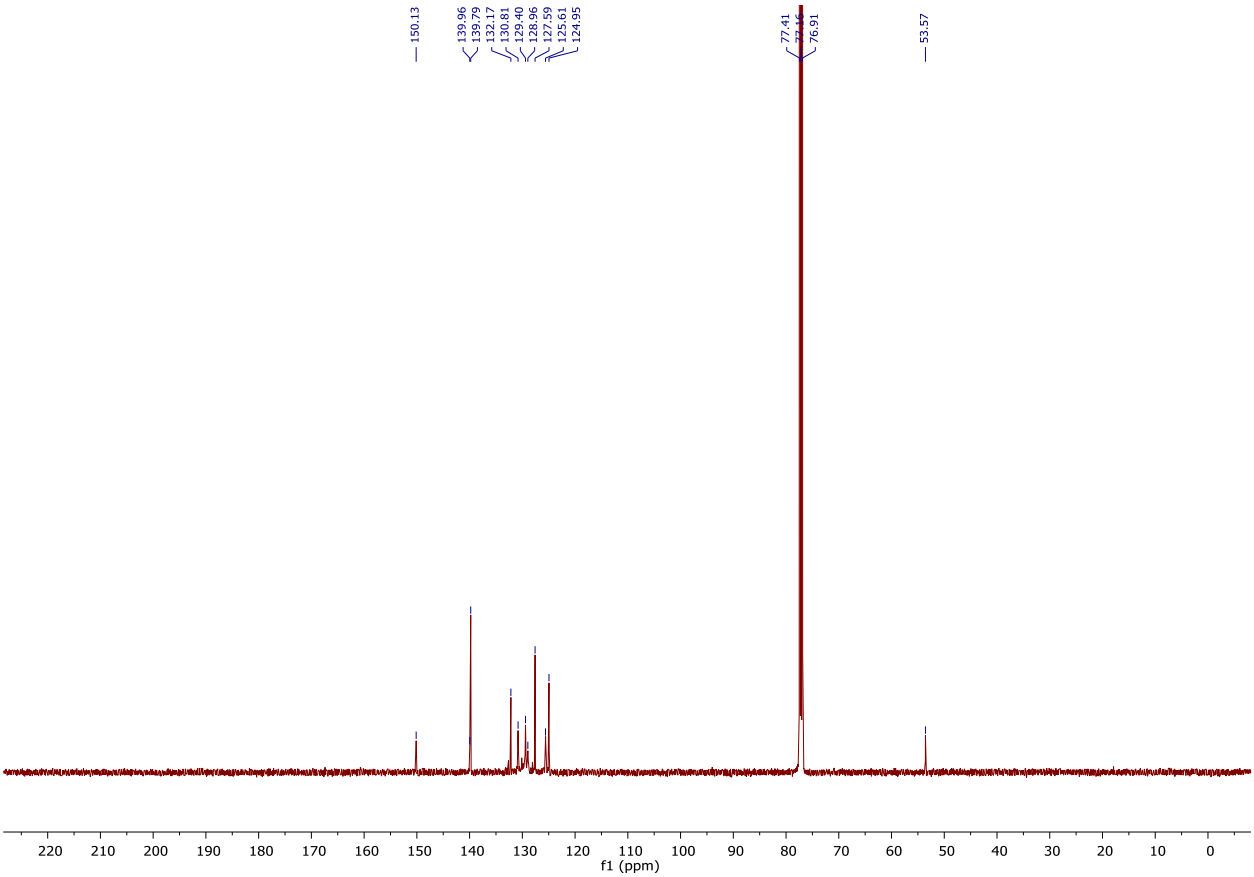

2,2'-bis(6-(1H-imidazol-1-yl)pyridin-2-yl)-1,1'-biphenyl

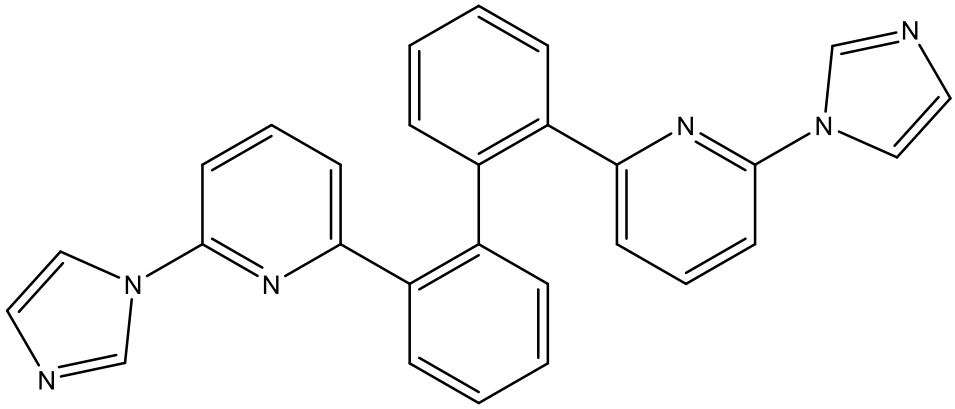

In a dry 2-neck 100 mL round bottom flask, sulfonyl diimidazole (0.8735 g, 4.407 mmol) is combined with dry chlorobenzene (10 mL) and set up under reflux. Another 100 mL 2-neck

round bottom flask with vacuum dried 2,2'-([1,1'-biphenyl]-2,2'-diyl)bis(pyridine 1-oxide) (0.5000 g, 1.469 mmol) was sealed and purged with nitrogen. Dry chlorobenzene (20 mL) was added to dissolve the solid. The solution was then added to the flask under reflux. Excess dry chlorobenzene was used to wash the extra product from the flask. The mixture was then heated to 130 °C for 6 days.[51]

2,2'-bis(6-(3-methyl-1H-3l4-imidazol-1-yl)pyridin-2-yl)-1,1'-biphenyl

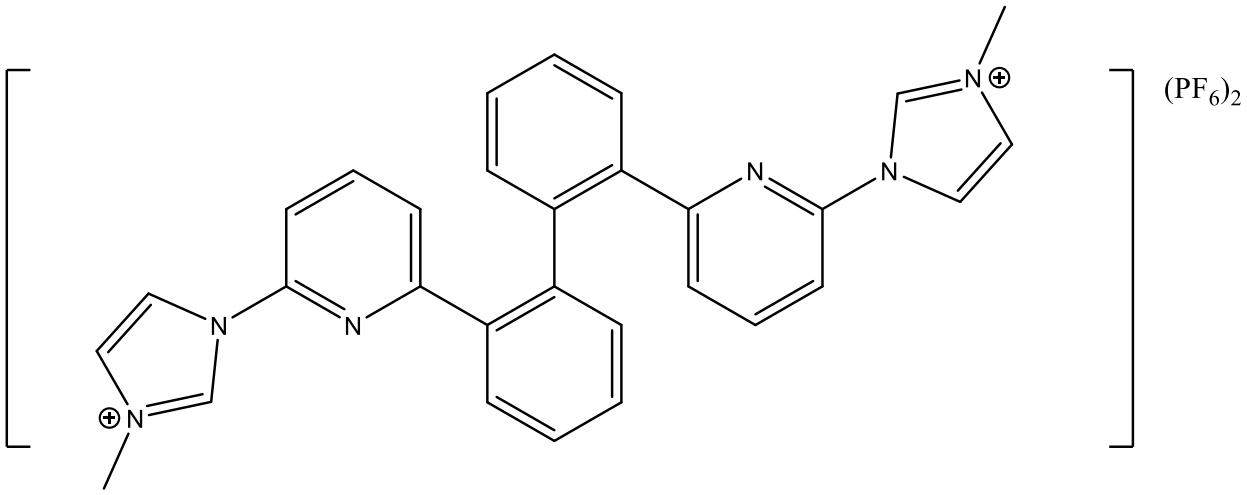

In a dry 100 mL 2-neck round bottom flask, 2,2'-bis(6-(1H-imidazol-1-yl)pyridin-2-yl)-1,1'-biphenyl (0.0910 g, 0.2066 mmol) and acetonitrile (50 mL) were combined. A reflux condenser was attached and the entire vessel was purged with nitrogen. Methyl iodide (0.13 mL, 2.066 mmol) was added dropwise. The mixture was then heated to 80 °C overnight. The reaction was cooled to room temperature and excess diethyl ether was added.[54]

[Ni(HD$_2$)]$^{2+}$

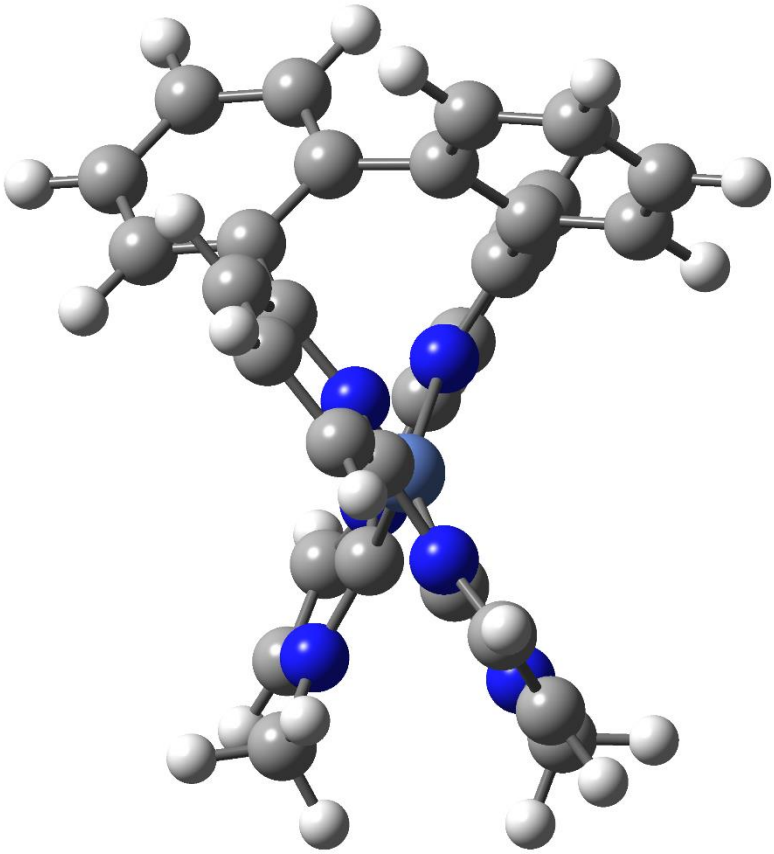

A DFT calculation for [Ni(HD1)](PF$_6$)$_2$ was done as a preliminary result to investigate the difference in bite angle that would be observed when changing the order of the donors in HD1 and HD2. DFT shows a bite angle of the catalyst to be 48.9°. The Chang catalysts led us to believe that these two potential catalysts would likely have different levels of reactivity.

[Ni(HD2)](PF$_6$)$_2$

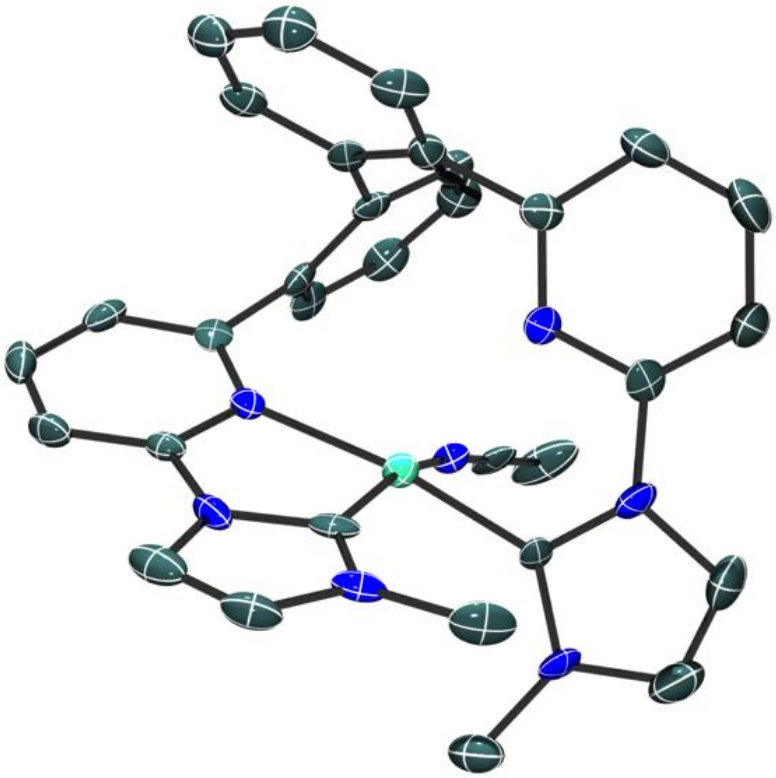

In a 20 mL screw cap glass vial, HD_2 (0.1000 g, 0.131 mmol) and acetonitrile (10 mL) were combined with five equivalents of Silver (I) Oxide (0.1518 g, 0.655 mmol). The vial was purged with nitrogen and stirred at room temperature overnight. The solution was then centrifuged and the pellet was removed. The solution was then placed in a new 20 mL screw cap glass vial along with one equivalent of $Ni(DME)Cl_2$ (0.0288 g, 0.132 mmol) was added to the solution. The vial was purged with nitrogen and stirred at room temperature overnight for transmetallation. The solution was then centrifuged again and the pellet was removed. The solution was then placed in yet another new 20 mL screw cap glass vial along with one equivalent of $NaPF_6$ (0.0220 g, 0.131 mmol) and stirred at room temperature overnight to achieve salt metathesis. Single crystals were obtained using ether diffusion into a concentrated

acetonitrile solution. It should be noted that the crystal structure is found to be 4-cooridinate, but that acetonitrile is coordinated. This differs from the DFT calculations and therefore yields a square planar geometry at the nickel center.[37,39]

ELECTROCHEMICAL STUDIES

HD_2Ni (1)

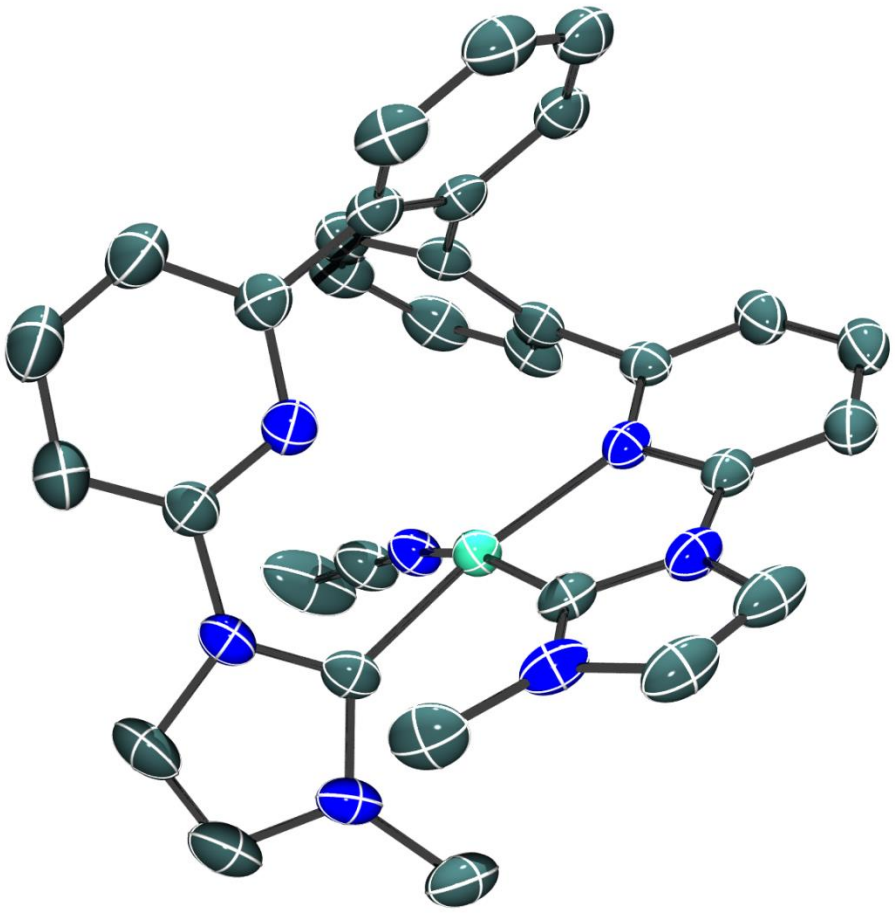

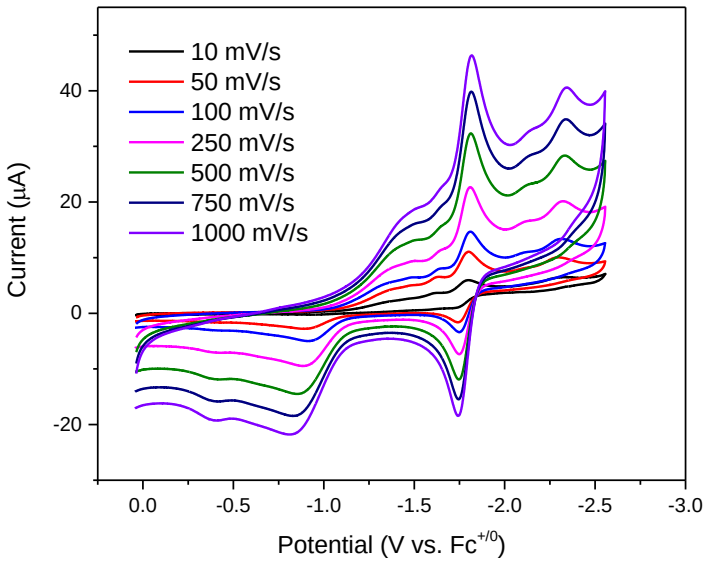

Figure 17: Cyclic voltammogram scan rate dependence of 1 mM **1** under an argon atmosphere in 0.1 M $TBAPF_6$/MeCN. A glassy carbon working electrode was used with a platinum wire counter electrode. A platinum wire was also used as a quasi-reference electrode. Ferrocene was added at the end of experiments as an internal standard.

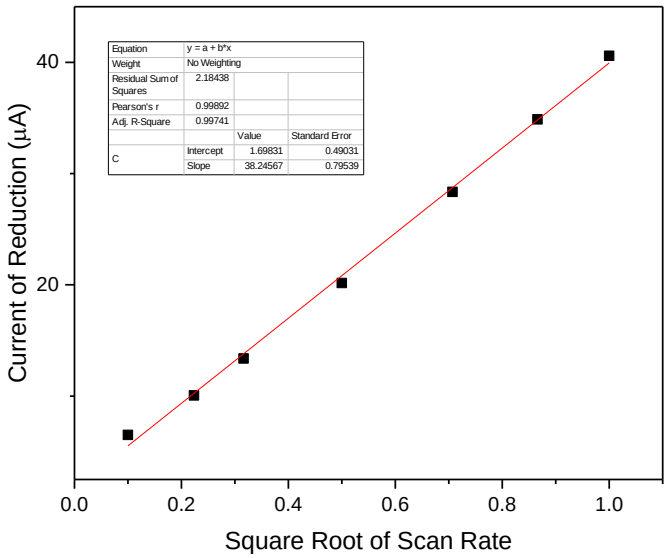

Figure 18: Scan rate dependence: Plot of reductive peak current in cyclic voltammograms from Figure 17 versus square root of scan rate. A linear fit is observed, consistent was a diffusional system.

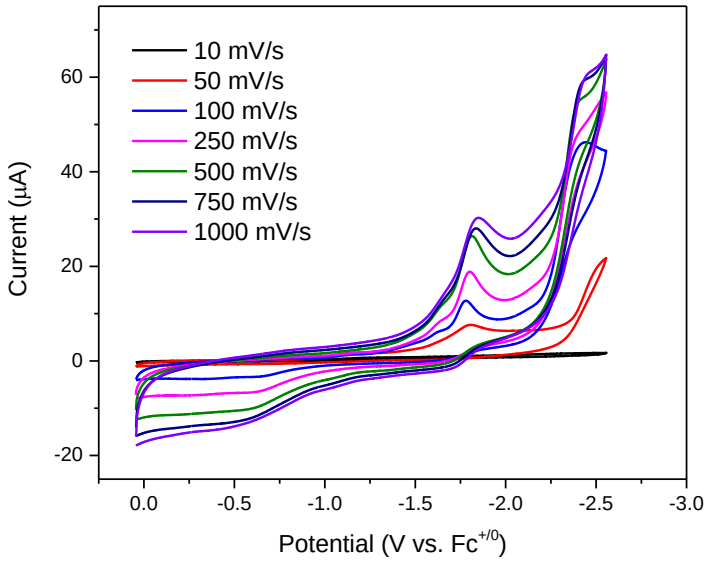

Figure 19: Cyclic voltammograms of 1 mM **1** under a carbon dioxide atmosphere in 0.1 M $TBAPF_6$/MeCN. A glassy carbon working electrode was used with a platinum wire counter electrode. A platinum wire was also used as a quasi-reference electrode. Ferrocene was added at the end of experiments as an internal standard.

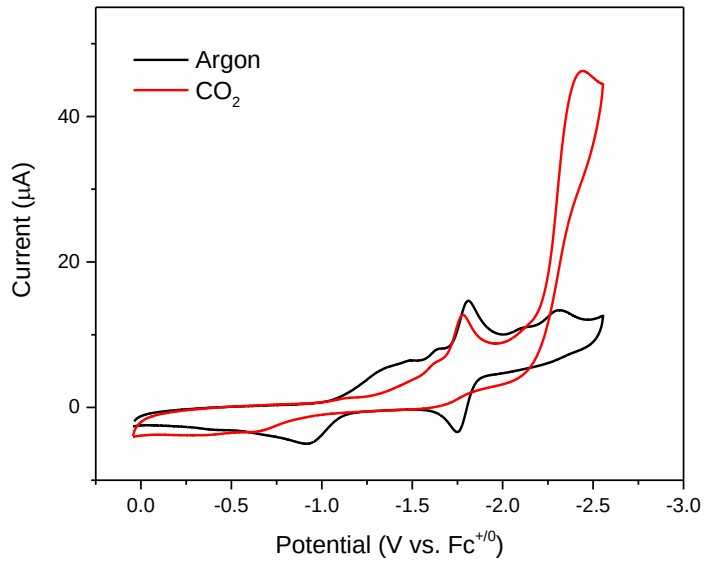

Figure 20: Cyclic voltammograms of 1 mM **1** under an argon (black) and carbon dioxide (red) atmosphere in 0.1 M $TBAPF_6$/MeCN. A glassy carbon working electrode was used with a platinum wire counter electrode. A platinum wire was also used as a quasi-reference electrode. Ferrocene was added at the end of experiments as an internal standard.

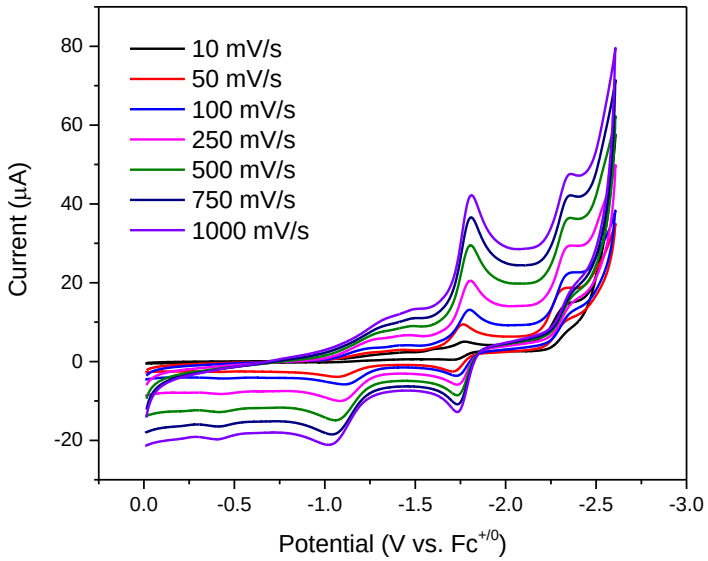

Figure 21: Cyclic voltammograms of 1 mM **1** under an argon atmosphere in 0.1 M $TBAPF_6$/MeCN with 2 M H_2O added as a proton source. A glassy carbon working electrode was used with a platinum wire counter electrode. A platinum wire was also used as a quasi-reference electrode. Ferrocene was added at the end of experiments as an internal standard.

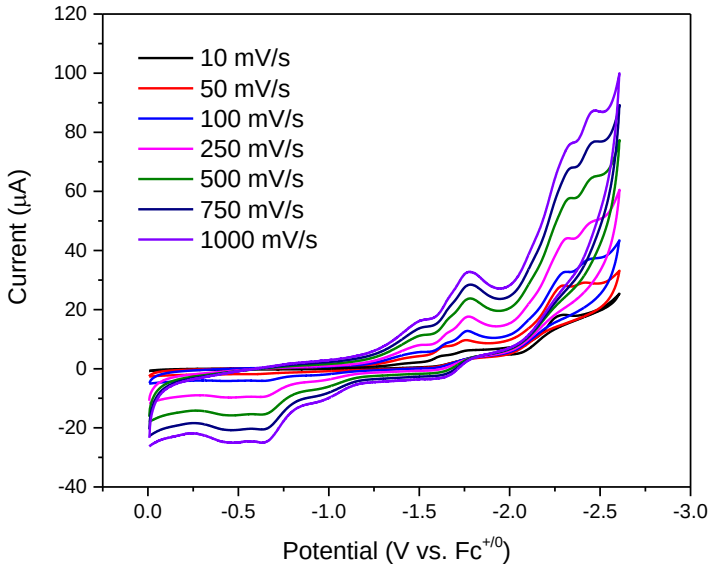

Figure 22: Cyclic voltammograms of 1 mM **1** under a carbon dioxide atmosphere in 0.1 M $TBAPF_6$/MeCN with 2 M H_2O added as a proton source. A glassy carbon working electrode was used with a platinum wire counter electrode. A platinum wire was also used as a quasi-reference electrode. Ferrocene was added at the end of experiments as an internal standard.

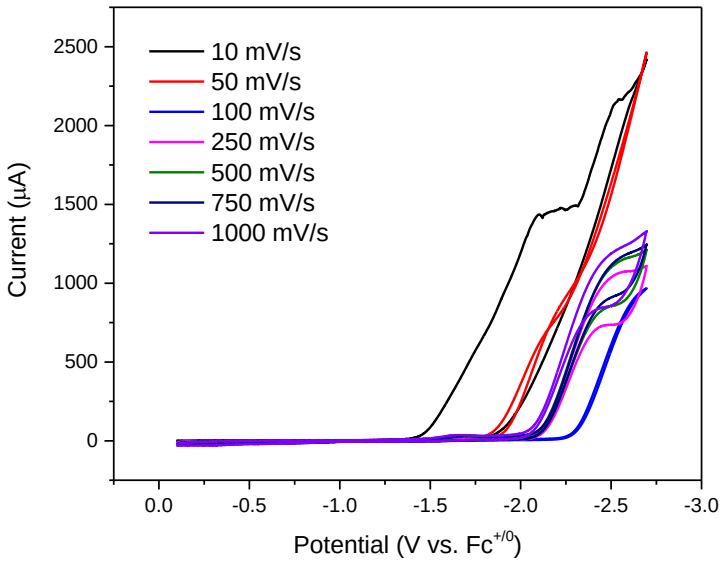

Figure 23: Cyclic voltammograms of 1 mM **1** under an argon atmosphere in 0.1 M $TBAPF_6$/MeCN with 1 M TFE added as a proton source. A glassy carbon working electrode was used with a platinum wire counter electrode. A platinum wire was also used as a quasi-reference electrode. Ferrocene was added at the end of experiments as an internal standard.

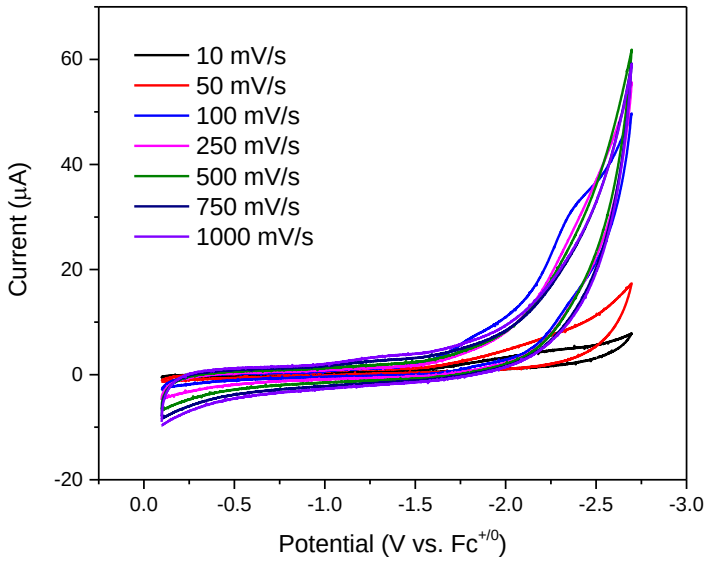

Figure 24: Cyclic voltammograms of 1 mM **1** under a carbon dioxide atmosphere in 0.1 M $TBAPF_6$/MeCN with 1 M TFE added as a proton source. A glassy carbon working electrode was used with a platinum wire counter electrode. A platinum wire was also used as a quasi-reference electrode. Ferrocene was added at the end of experiments as an internal standard.

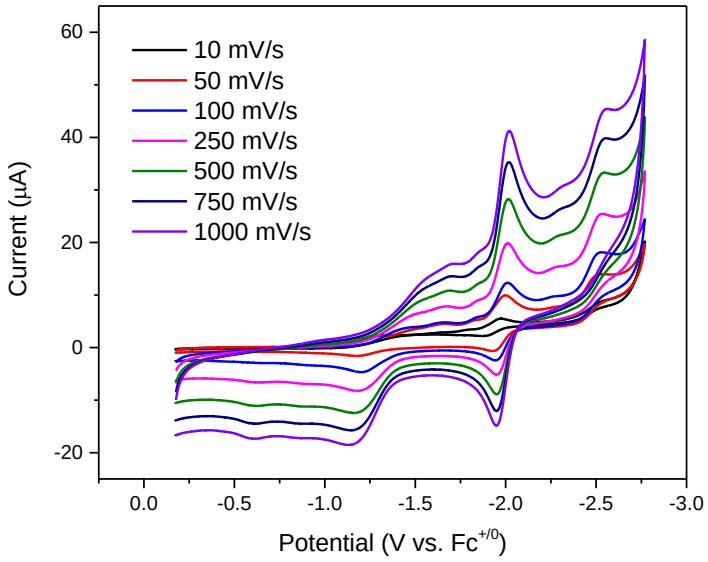

Figure 25: Cyclic voltammograms of 1 mM **1** under an argon atmosphere in 0.1 M $TBAPF_6$/MeCN with 1 M MeOH added as a proton source. A glassy carbon working electrode was used with a platinum wire counter electrode. A platinum wire was also used as a quasi-reference electrode. Ferrocene was added at the end of experiments as an internal standard.

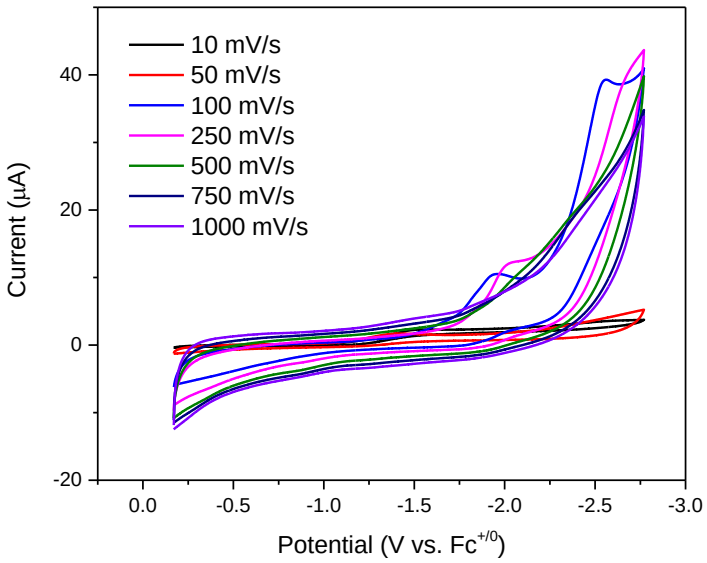

Figure 26: Cyclic voltammograms of 1 mM **1** under a carbon dioxide atmosphere in 0.1 M $TBAPF_6$/MeCN with 1 M MeOH added as a proton source. A glassy carbon working electrode was used with a platinum wire counter electrode. A platinum wire was also used as a quasi-reference electrode. Ferrocene was added at the end of experiments as an internal standard.

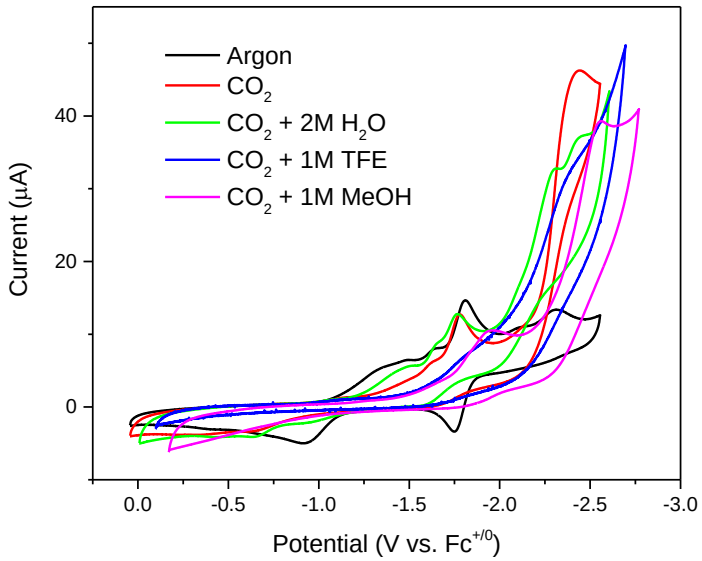

Figure 27: Cyclic voltammogram at 100 mV/s scan rate of 1 mM **1** under argon and carbon dioxide atmosphere in 0.1 M $TBAPF_6$/MeCN. TFE (1 M), H_2O (2 M), and MeOH (1 M) were used as proton sources. A glassy carbon working electrode was used with a platinum wire counter electrode. A platinum wire was also used as a quasi-reference electrode. Ferrocene was added as an internal standard.

Proton Source	$[H^+]$	i_p Peak 2	i_{cat} Peak 2	$(i_{cat}/i_p)^2$ Peak 2	TOF (s^{-1}) Peak 2
None	—	13.3699	46.2500	11.9665	2.3193
H_2O	2M	22.6382	37.4761	2.7405	0.5311
TFE	1M				
MeOH	1M	18.1429	39.2919	4.6902	0.9090

Table 3: All peak currents taken using 100 mV/s scan rates. Tabulated results of **1** utilizing various proton sources. These results were obtained from the cyclic voltammagrams shown above. The calculations for turnover frequency were done using the equation proposed by the Kubiak Group.[45] Calculations for TFE were unable to be completed due to a large response by the catalyst under the argon environment.

Electrochemical studies were performed on **1** to test for its catalytic properties. The catalytic system was found to be diffusional, given the high R^2 value when the reduction potentials were plotted vs the square root of the scan rate. The catalyst showed mild activity under a catalytic atmosphere of carbon dioxide. This increase in current under the catalytic

environment can be seen in comparison to the neutral environment in Figure 20. The catalytically active reduction does occur at a very negative potential. This is less than favorable, but the activity shown under the catalytic atmosphere is worth further investigation.

The catalyst was also investigated with different common proton sources. A comparison of the catalyst with these proton sources under a catalytic environment and the catalyst under a non-catalytic environment. This comparison can be seen in Figure 27. The catalyst shows a decrease in activity when the proton source is introduced. This suggests that their might be competing reactions occurring in the presence of a proton source. Further investigation will need to be done utilizing a gas chromatograph in order to discover the efficiency and selectivity of this catalyst.

Lizhu's complex (2)

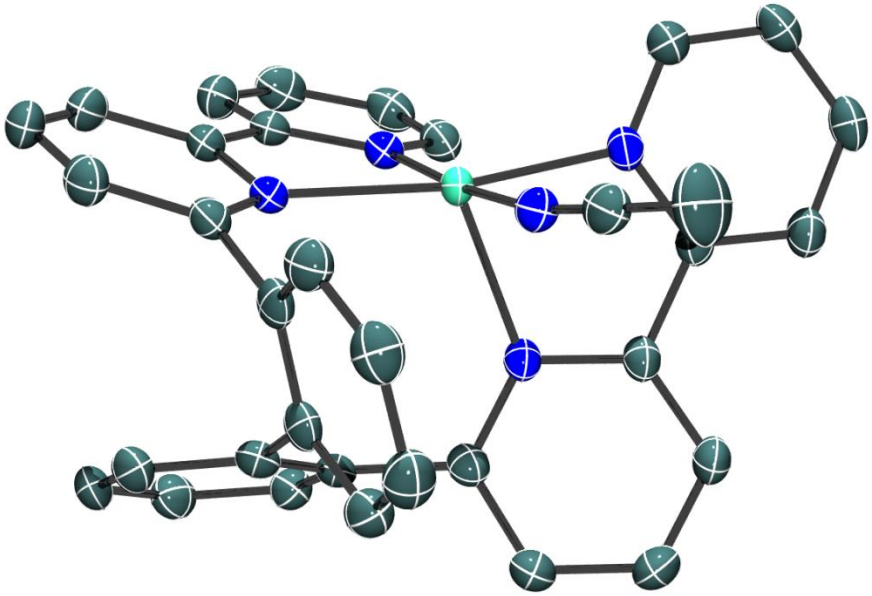

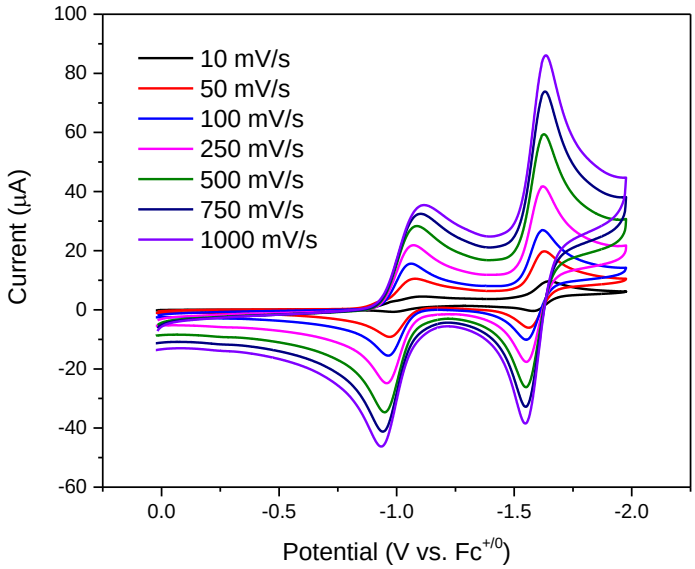

Figure 28: Cyclic voltammogram scan rate dependence of 1 mM **2** under an argon atmosphere in 0.1 M $TBAPF_6$/MeCN. A glassy carbon working electrode was used with a platinum wire counter electrode. A platinum wire was also used as a quasi-reference electrode. Ferrocene was added at the end of experiments as an internal standard.

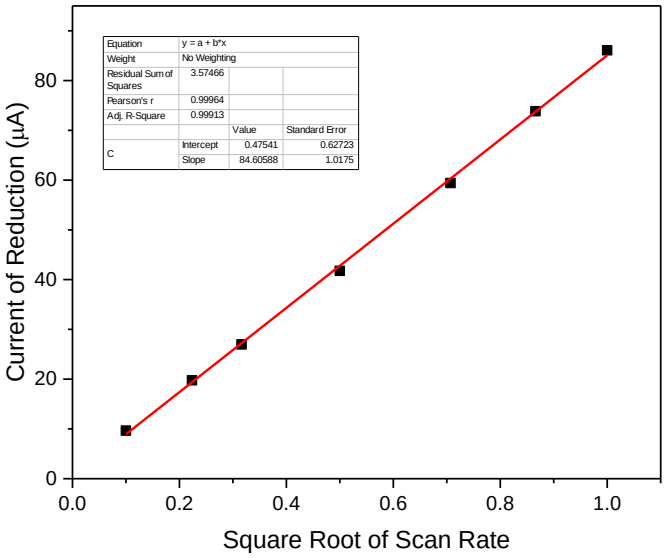

Figure 29: Scan rate dependence: Plot of reductive peak current in cyclic voltammograms from Figure 28 versus square root of scan rate. A linear fit is observed, consistent was a diffusional system.

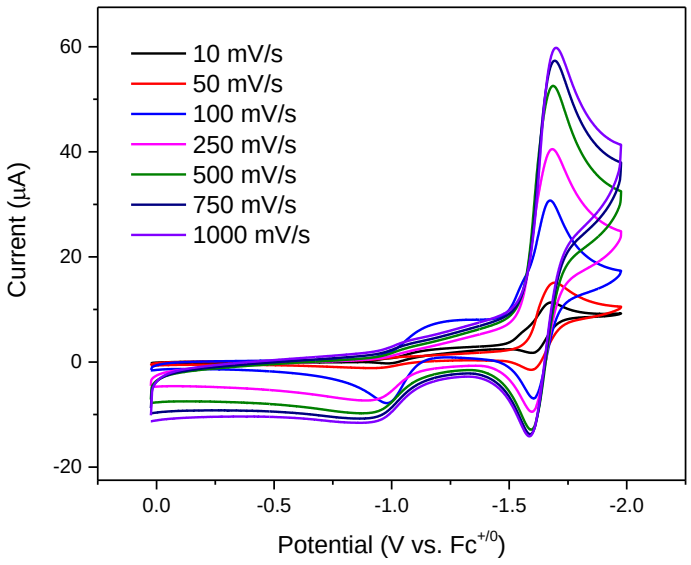

Figure 30: Cyclic voltammograms of 1 mM **2** under a carbon dioxide atmosphere in 0.1 M $TBAPF_6$/MeCN. A glassy carbon working electrode was used with a platinum wire counter electrode. A platinum wire was also used as a quasi-reference electrode. Ferrocene was added at the end of experiments as an internal standard.

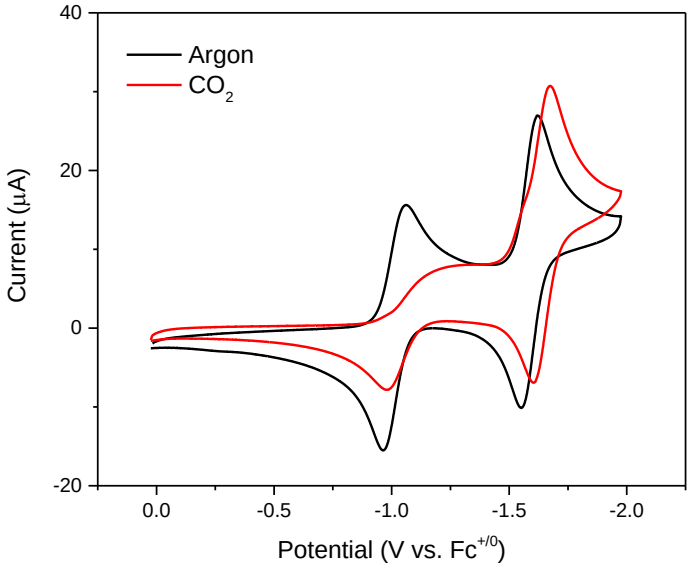

Figure 31: Cyclic voltammograms of 1 mM **2** under an argon (black) and carbon dioxide (red) atmosphere in 0.1 M $TBAPF_6$/MeCN. A glassy carbon working electrode was used with a platinum wire counter electrode. A platinum wire was also used as a quasi-reference electrode. Ferrocene was added at the end of experiments as an internal standard.

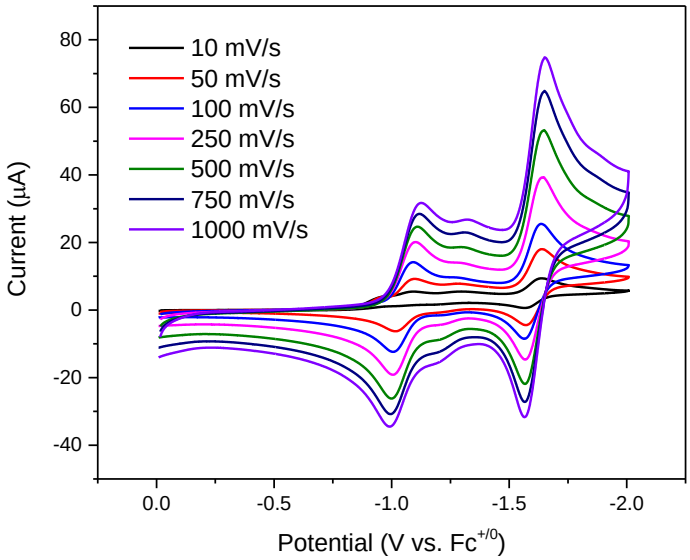

Figure 32: Cyclic voltammograms of 1 mM **2** under an argon atmosphere in 0.1 M $TBAPF_6$/MeCN with 2 M H_2O added as a proton source. A glassy carbon working electrode was used with a platinum wire counter electrode. A platinum wire was also used as a quasi-reference electrode. Ferrocene was added at the end of experiments as an internal standard.

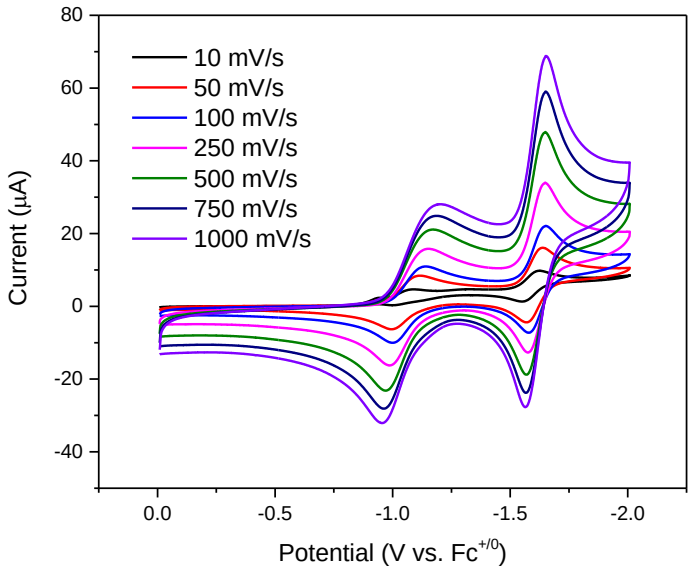

Figure 33: Cyclic voltammograms of 1 mM **2** under a carbon dioxide atmosphere in 0.1 M $TBAPF_6$/MeCN with 2 M H_2O added as a proton source. A glassy carbon working electrode was used with a platinum wire counter electrode. A platinum wire was also used as a quasi-reference electrode. Ferrocene was added at the end of experiments as an internal standard.

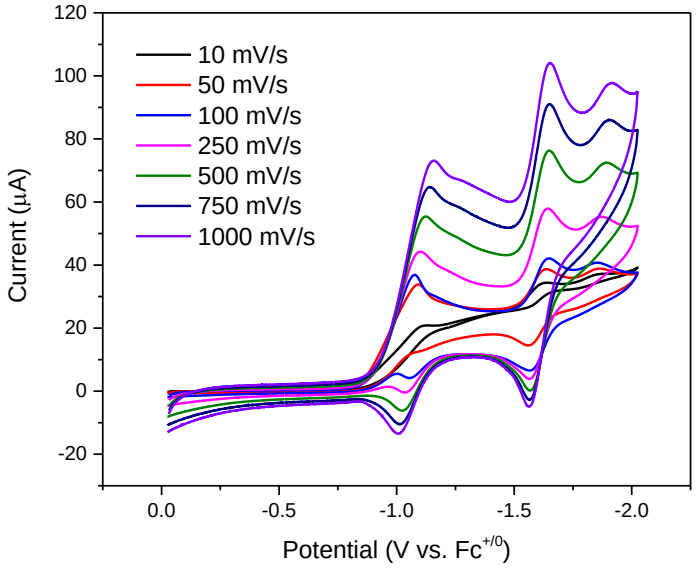

Figure 34: Cyclic voltammograms of 1 mM **2** under an argon atmosphere in 0.1 M $TBAPF_6$/MeCN with 1 M TFE added as a proton source. A glassy carbon working electrode was used with a platinum wire counter electrode. A platinum wire was also used as a quasi-reference electrode. Ferrocene was added at the end of experiments as an internal standard.

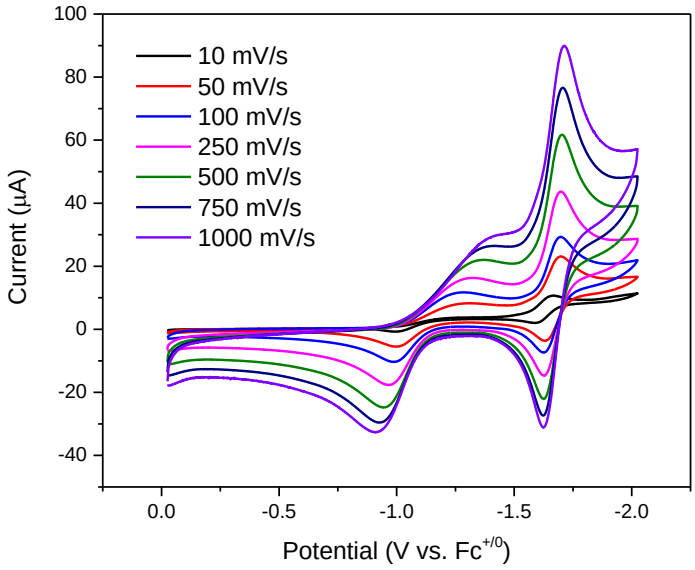

Figure 35: Cyclic voltammograms of 1 mM **2** under a carbon dioxide atmosphere in 0.1 M $TBAPF_6$/MeCN with 1 M TFE added as a proton source. A glassy carbon working electrode was used with a platinum wire counter electrode. A platinum wire was also used as a quasi-reference electrode. Ferrocene was added at the end of experiments as an internal standard.

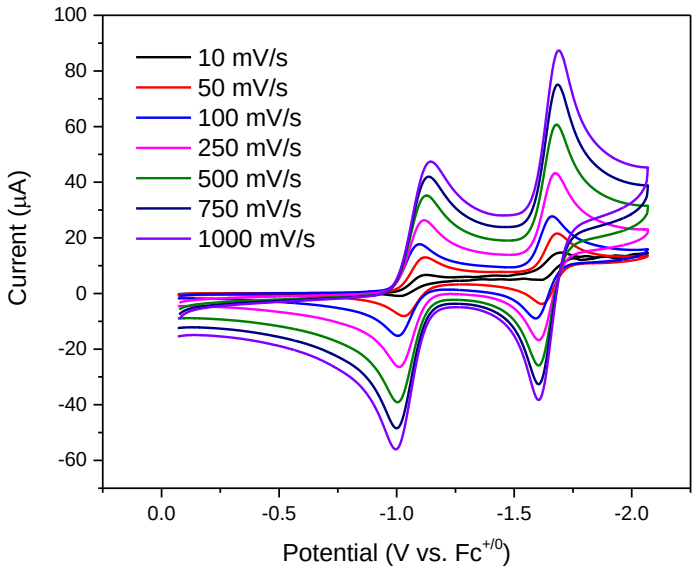

Figure 36: Cyclic voltammograms of 1 mM **2** under an argon atmosphere in 0.1 M $TBAPF_6$/MeCN with 1 M MeOH added as a proton source. A glassy carbon working electrode was used with a platinum wire counter electrode. A platinum wire was also used as a quasi-reference electrode. Ferrocene was added at the end of experiments as an internal standard.

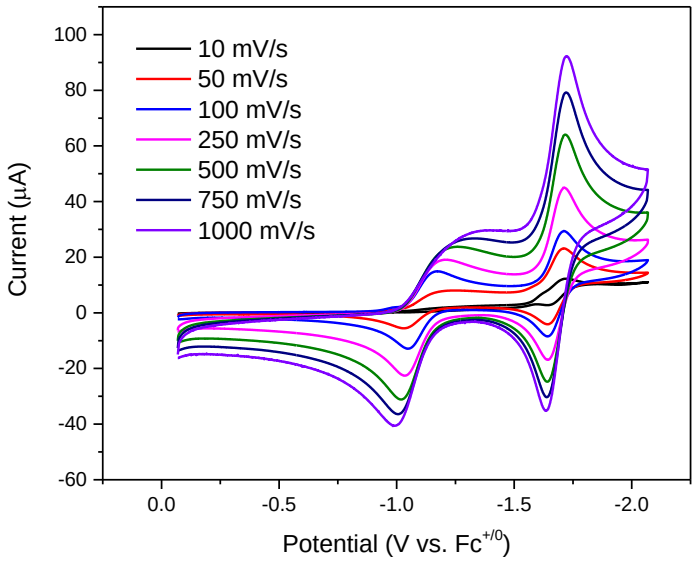

Figure 37: Cyclic voltammograms of 1 mM **2** under a carbon dioxide atmosphere in 0.1 M $TBAPF_6$/MeCN with 1 M MeOH added as a proton source. A glassy carbon working electrode was used with a platinum wire counter electrode. A platinum wire was also used as a quasi-reference electrode. Ferrocene was added at the end of experiments as an internal standard.

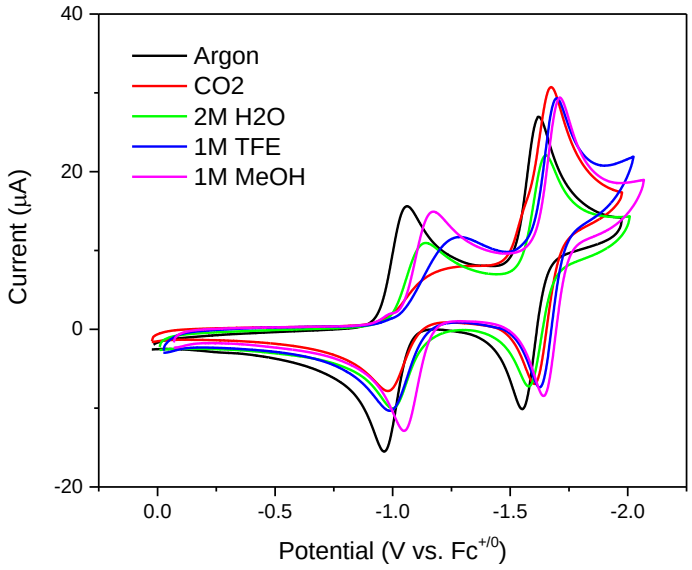

Figure 38: Cyclic voltammogram at 100 mV/s scan rate of 1 mM **2** under argon and carbon dioxide atmosphere in 0.1 M $TBAPF_6$/MeCN. TFE (1 M), H_2O (2 M), and MeOH (1 M) were used as proton sources. A glassy carbon working electrode was used with a platinum wire counter electrode. A platinum wire was also used as a quasi-reference electrode. Ferrocene was added as an internal standard.

Proton Source	$[H^+]$	i_p Peak 2	i_{cat} Peak 2	$(i_{cat}/i_p)^2$ Peak 2	TOF (s^{-1}) Peak 2
None	—	26.9657	30.7347	1.2991	0.2518
H_2O	2M	25.4978	22.1133	0.7521	0.1458
TFE	1M	42.1149	29.3125	0.4844	0.0939
MeOH	1M	27.7225	29.4163	1.1259	0.2182

Table 4: All peak currents taken using 100 mV/s scan rates. Tabulated results of **2** utilizing various proton sources. These results were obtained from the cyclic voltammagrams shown above. The calculations for turnover frequency were done using the equation proposed by the Kubiak group.[45]

Electrochemical studies were performed on **2** to test for its catalytic properties. The catalytic system was found to be diffusional, given the high R^2 value when the reduction potentials were plotted vs the square root of the scan rate. The catalyst showed very low activity under a catalytic atmosphere of carbon dioxide. This small increase in current under the catalytic environment can be seen in comparison to the neutral environment in Figure 31. The catalytically active reduction does occur at a much less negative potential than **1**. This is much more favorable, but the activity shown under the catalytic atmosphere makes it questionable for further investigation.

The catalyst was also investigated with different common proton sources. A comparison of the catalyst with these proton sources under a catalytic environment and the catalyst under a non-catalytic environment. This comparison can be seen in Figure 38. The catalyst shows

virtually no change in activity when the proton source is introduced. There is some plateauing of the catalytic peak which could suggest some activity at slower scan rates. Further investigation will need to be done utilizing a gas chromatograph in order to discover the efficiency and selectivity of this catalyst.

Dr. Jurss' complex (3)

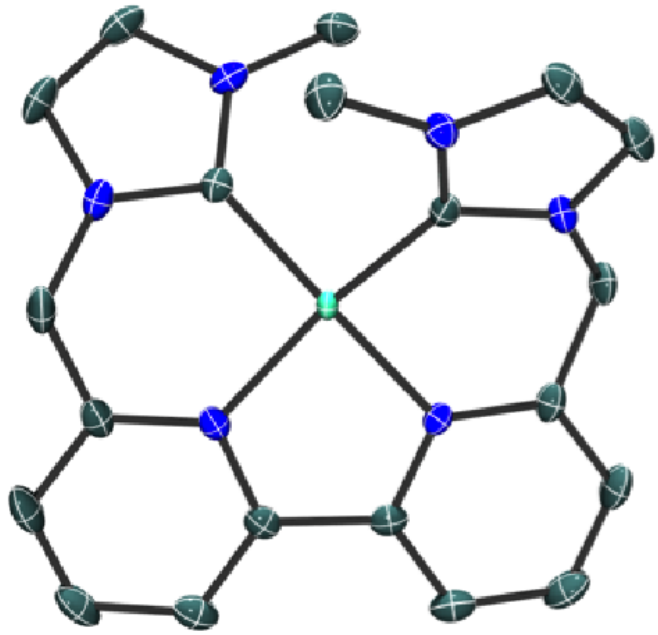

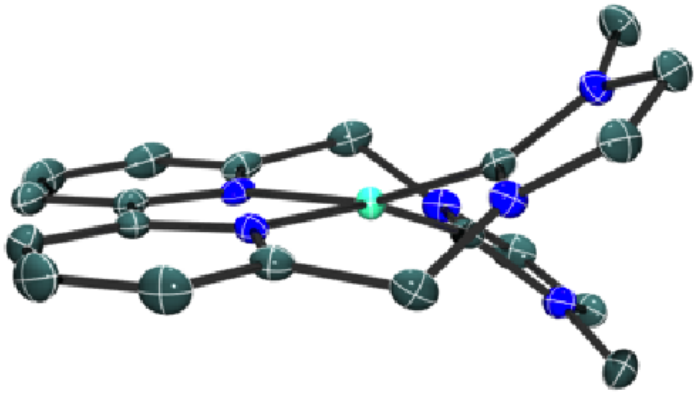

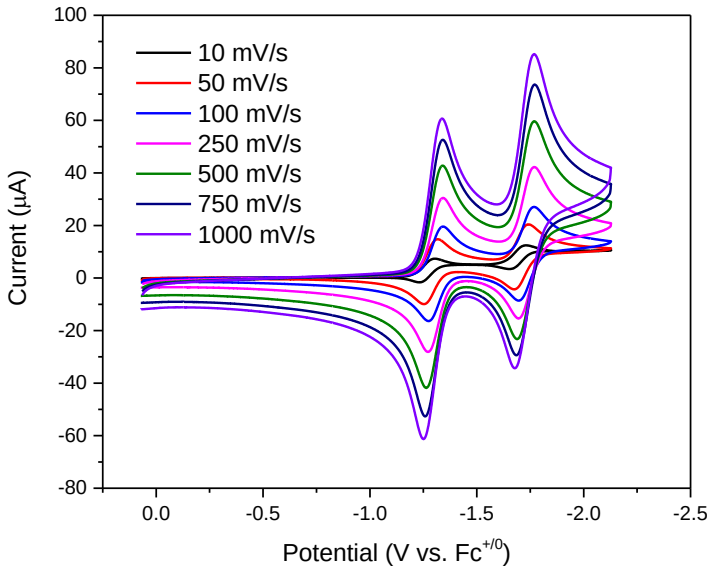

Figure 39: Cyclic voltammogram scan rate dependence of 1 mM **3** under an argon atmosphere in 0.1 M $TBAPF_6$/MeCN. A glassy carbon working electrode was used with a platinum wire counter electrode. A platinum wire was also used as a quasi-reference electrode. Ferrocene was added at the end of experiments as an internal standard.

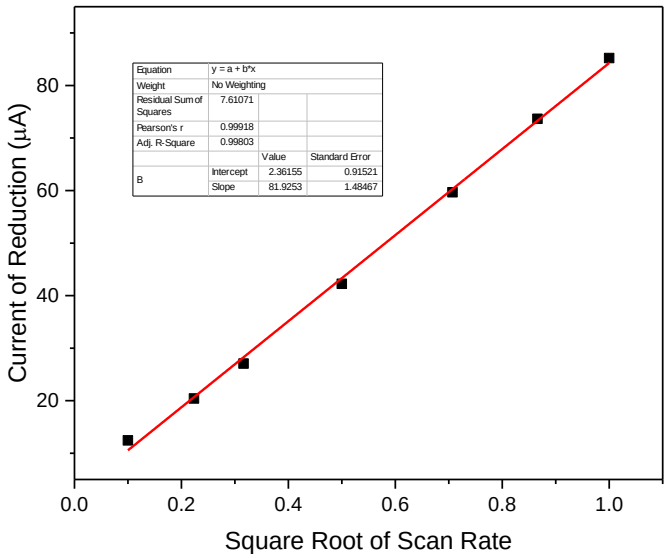

Figure 40: Scan rate dependence: Plot of reductive peak current in cyclic voltammograms from Figure 39 versus square root of scan rate. A linear fit is observed, consistent was a diffusional system.

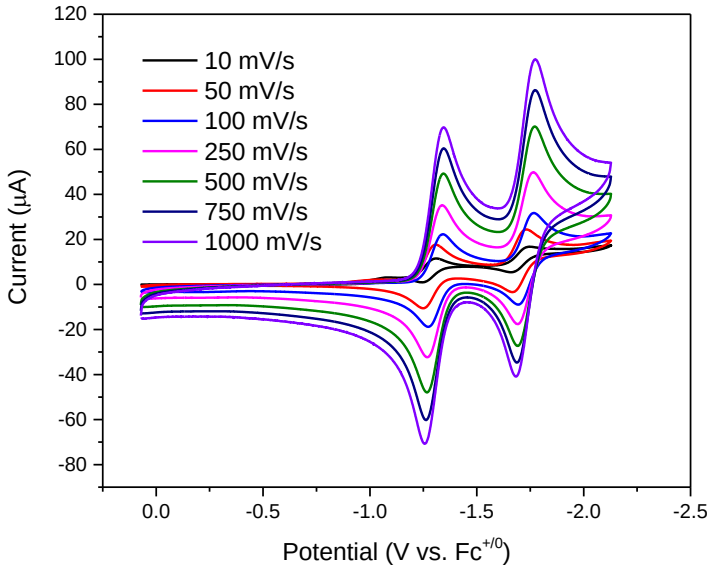

Figure 41: Cyclic voltammograms of 1 mM **3** under a carbon dioxide atmosphere in 0.1 M $TBAPF_6$/MeCN. A glassy carbon working electrode was used with a platinum wire counter electrode. A platinum wire was also used as a quasi-reference electrode. Ferrocene was added at the end of experiments as an internal standard.

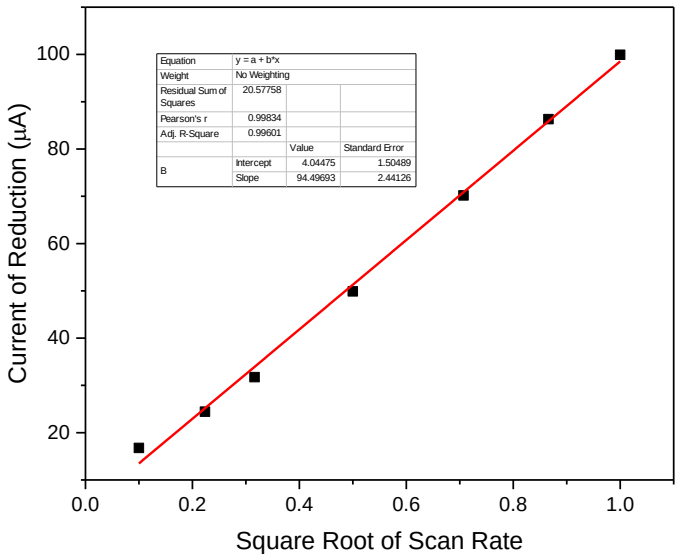

Figure 42: Scan rate dependence: Plot of reductive peak current in cyclic voltammograms from Figure 41 versus square root of scan rate. A linear fit is observed, consistent was a diffusional system.

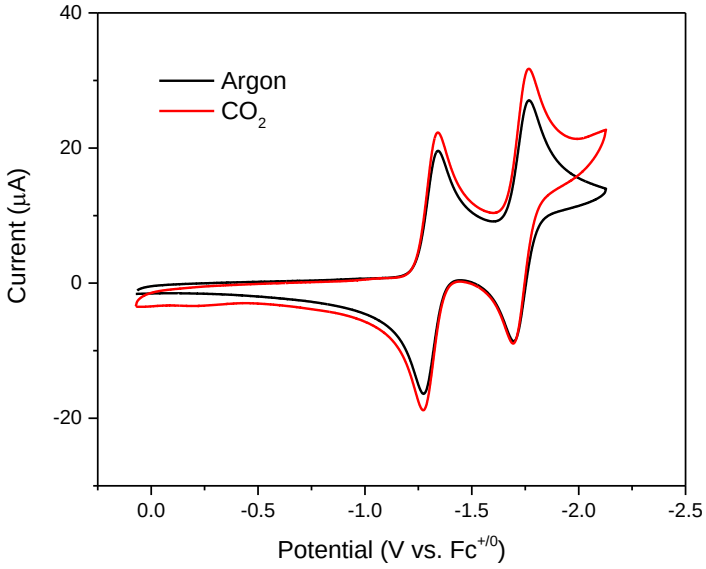

Figure 43: Cyclic voltammograms of 1 mM **3** under an argon (black) and carbon dioxide (red) atmosphere in 0.1 M $TBAPF_6$/MeCN. A glassy carbon working electrode was used with a platinum wire counter electrode. A platinum wire was also used as a quasi-reference electrode. Ferrocene was added at the end of experiments as an internal standard.

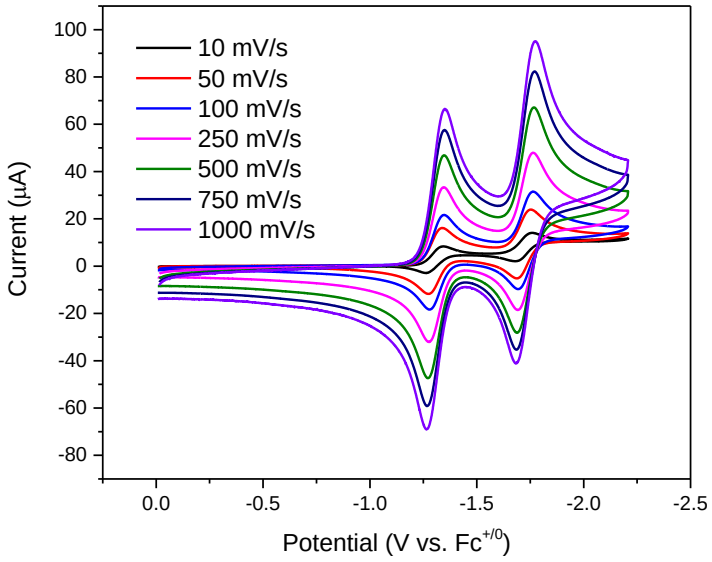

Figure 44: Cyclic voltammograms of 1 mM **3** under an argon atmosphere in 0.1 M $TBAPF_6$/MeCN with 2 M H_2O added as a proton source. A glassy carbon working electrode was used with a platinum wire counter electrode. A platinum wire was also used as a quasi-reference electrode. Ferrocene was added at the end of experiments as an internal standard.

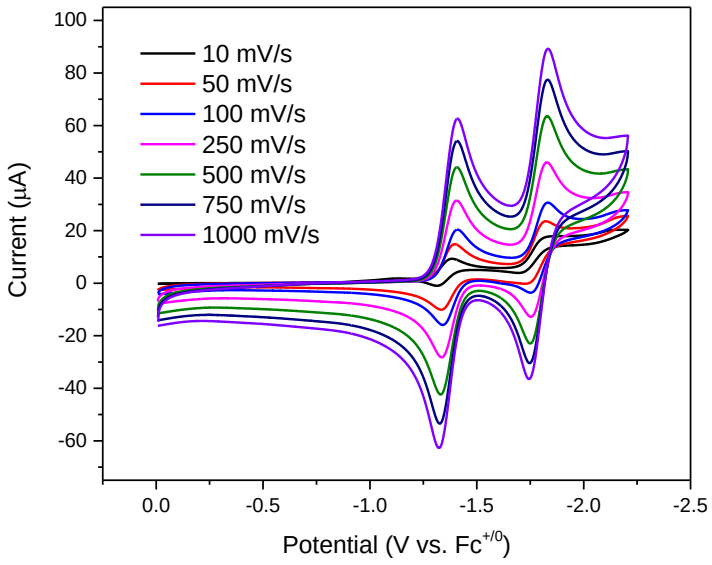

Figure 45: Cyclic voltammograms of 1 mM **3** under a carbon dioxide atmosphere in 0.1 M $TBAPF_6$/MeCN with 2 M H_2O added as a proton source. A glassy carbon working electrode was used with a platinum wire counter electrode. A platinum wire was also used as a quasi-reference electrode. Ferrocene was added at the end of experiments as an internal standard.

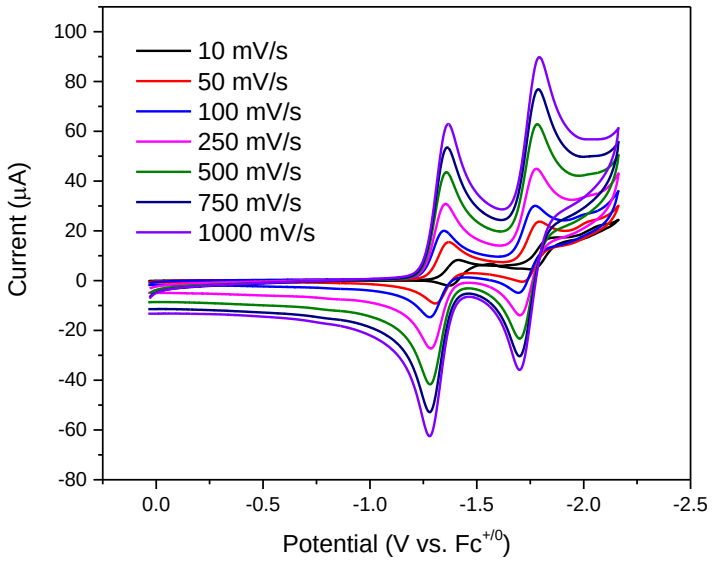

Figure 46: Cyclic voltammograms of 1 mM **3** under an argon atmosphere in 0.1 M $TBAPF_6$/MeCN with 1 M TFE added as a proton source. A glassy carbon working electrode was used with a platinum wire counter electrode. A platinum wire was also used as a quasi-reference electrode. Ferrocene was added at the end of experiments as an internal standard.

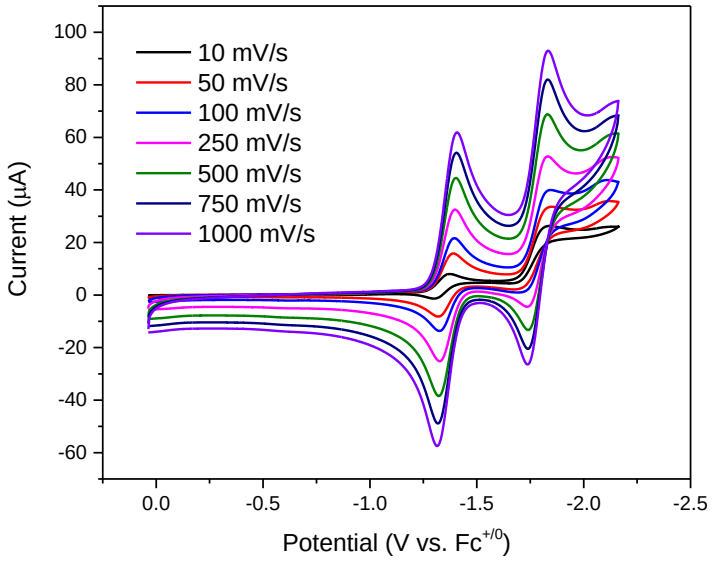

Figure 47: Cyclic voltammograms of 1 mM **3** under a carbon dioxide atmosphere in 0.1 M $TBAPF_6$/MeCN with 1 M TFE added as a proton source. A glassy carbon working electrode was used with a platinum wire counter electrode. A platinum wire was also used as a quasi-reference electrode. Ferrocene was added at the end of experiments as an internal standard.

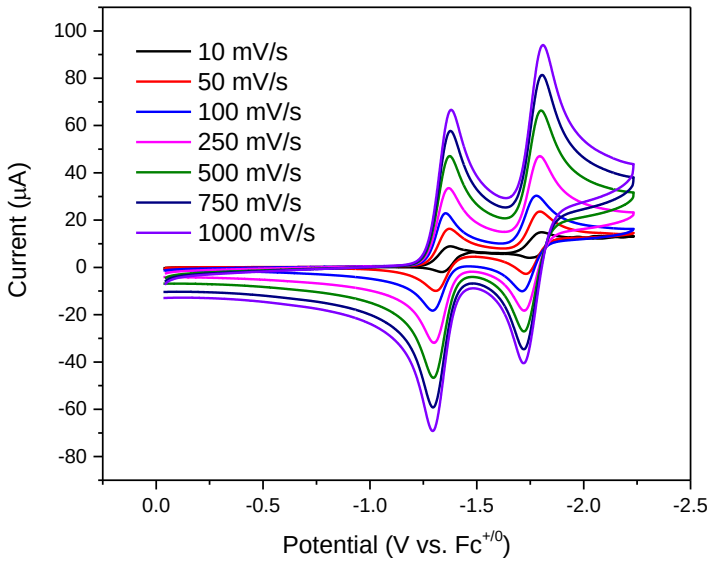

Figure 48: Cyclic voltammograms of 1 mM **3** under an argon atmosphere in 0.1 M $TBAPF_6$/MeCN with 1 M MeOH added as a proton source. A glassy carbon working electrode was used with a platinum wire counter electrode. A platinum wire was also used as a quasi-reference electrode. Ferrocene was added at the end of experiments as an internal standard.

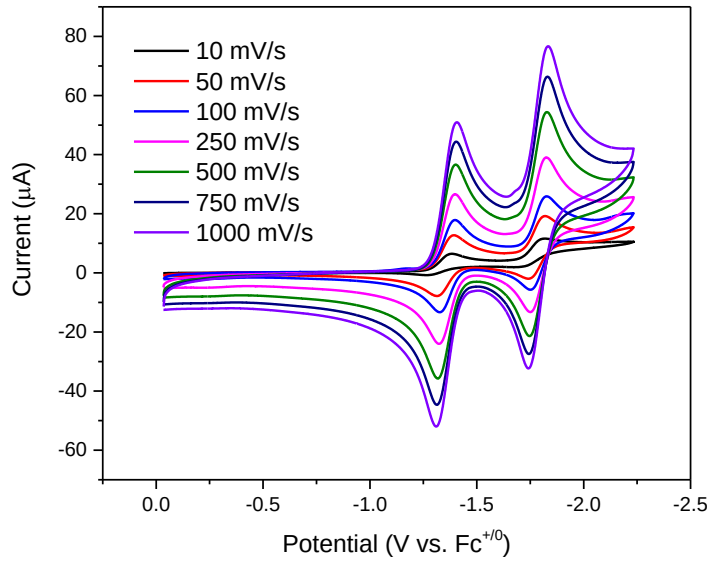

Figure 49: Cyclic voltammograms of 1 mM **3** under a carbon dioxide atmosphere in 0.1 M $TBAPF_6$/MeCN with 1 M MeOH added as a proton source. A glassy carbon working electrode was used with a platinum wire counter electrode. A platinum wire was also used as a quasi-reference electrode. Ferrocene was added at the end of experiments as an internal standard.

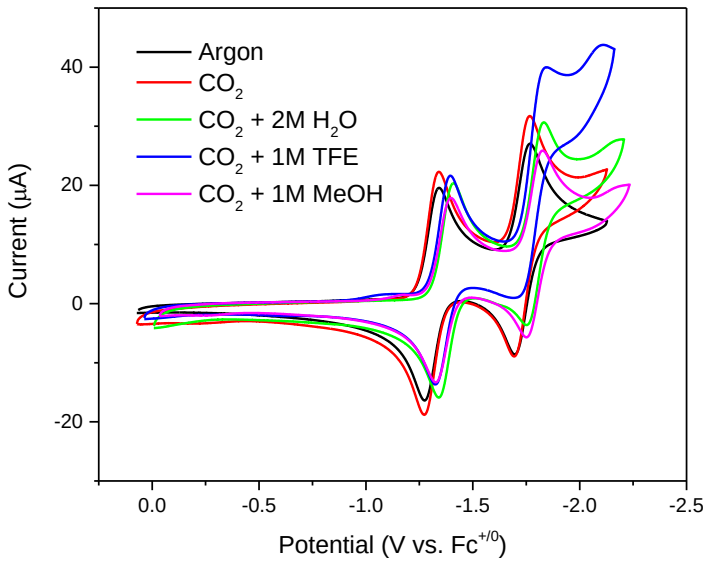

Figure 50: Cyclic voltammogram at 100 mV/s scan rate of 1 mM **3** under argon and carbon dioxide atmosphere in 0.1 M $TBAPF_6$/MeCN. TFE (1 M), H_2O (2 M), and MeOH (1 M) were used as proton sources. A glassy carbon working electrode was used with a platinum wire counter electrode. A platinum wire was also used as a quasi-reference electrode. Ferrocene was added as an internal standard.

Proton Source	[H^+]	i_p Peak 2	i_{cat} Peak 2	$(i_{cat}/i_p)^2$ Peak 2	TOF (s^{-1}) Peak 2
None	—	27.0695	31.7296	1.3739	0.2663
H_2O	2M	31.4915	30.6614	0.9480	0.1837
TFE	1M	30.0511	39.9847	1.7704	0.3431
MeOH	1M	30.3105	25.8854	0.7293	0.1413

Table 5: All peak currents taken using 100 mV/s scan rates. Tabulated results of **3** utilizing various proton sources. These results were obtained from the cyclic voltammagrams shown above. The calculations for turnover frequency were done using the equation proposed by the Kubiak group.[45]

Electrochemical studies were performed on **3** to test for its catalytic properties. The catalytic system was found to be diffusional, given the high R^2 value when the reduction potentials were plotted vs the square root of the scan rate. The catalyst showed very low activity under a catalytic atmosphere of carbon dioxide. This small increase in current under the catalytic environment can be seen in comparison to the neutral environment in Figure 43. There is some plateauing of the reduction peak under the catalytic atmosphere. The catalytically active reduction does occur at a much less negative potential than **1**. This is much more favorable, and the activity shown under the catalytic atmosphere makes it interesting for some further investigation.

The catalyst was also investigated with different common proton sources. A comparison of the catalyst with these proton sources under a catalytic environment and the catalyst under a

non-catalytic environment. This comparison can be seen in Figure 50. The catalyst shows some change in activity when the proton source is introduced, especially TFE. There is some plateauing of all of the catalytic peak which could suggest some activity at slower scan rates. Further investigation will need to be done utilizing a gas chromatograph in order to discover the efficiency and selectivity of this catalyst.

COLLABORATION WITH THE DELCAMP GROUP

Dr. Delcamp's complex (4)

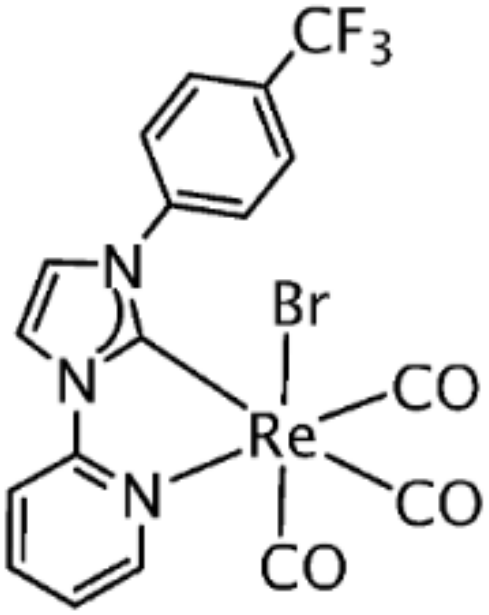

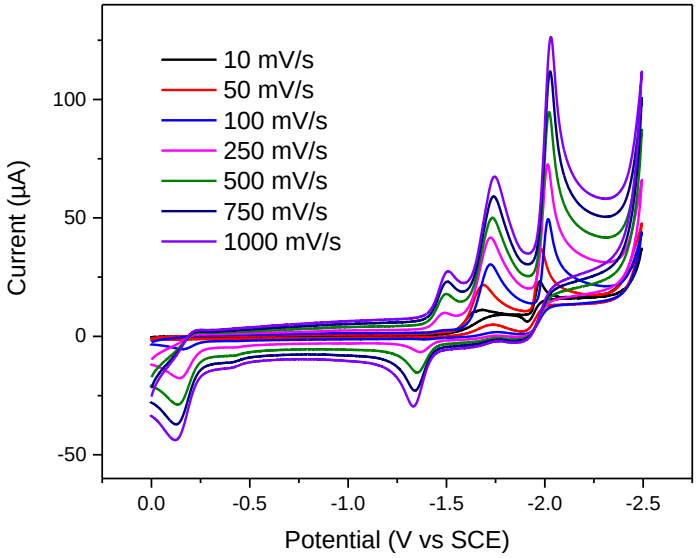

Figure 51: Cyclic voltammogram scan rate dependence of 1 mM **4** under an argon atmosphere in 0.1 M $TBAPF_6$/MeCN. A glassy carbon working electrode was used with a platinum wire counter electrode. A platinum wire was also used as a quasi-reference electrode. Ferrocene was added at the end of experiments as an internal standard.

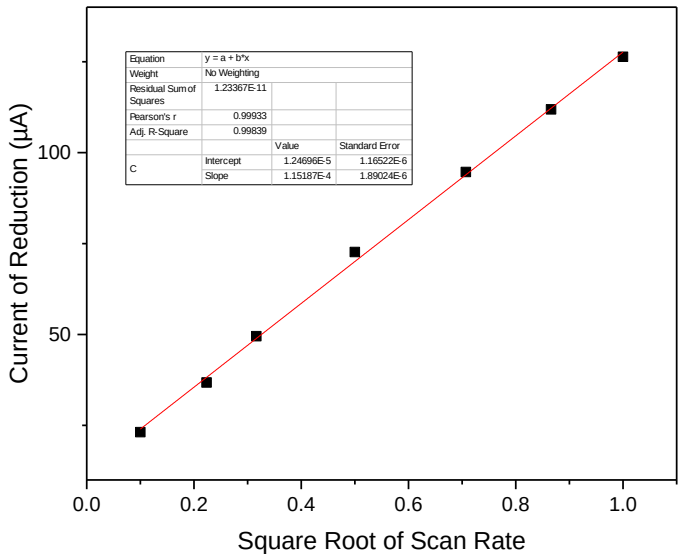

Figure 52: Scan rate dependence: Plot of reductive peak current in cyclic voltammograms from Figure 51 versus square root of scan rate. A linear fit is observed, consistent was a diffusional system.

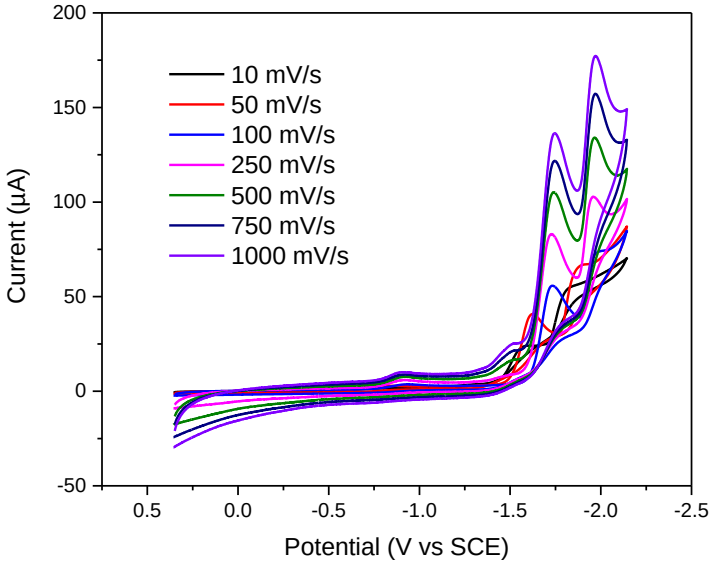

Figure 53: Cyclic voltammograms of 1 mM **4** under a carbon dioxide atmosphere in 0.1 M $TBAPF_6$/MeCN. A glassy carbon working electrode was used with a platinum wire counter electrode. A platinum wire was also used as a quasi-reference electrode. Ferrocene was added at the end of experiments as an internal standard.

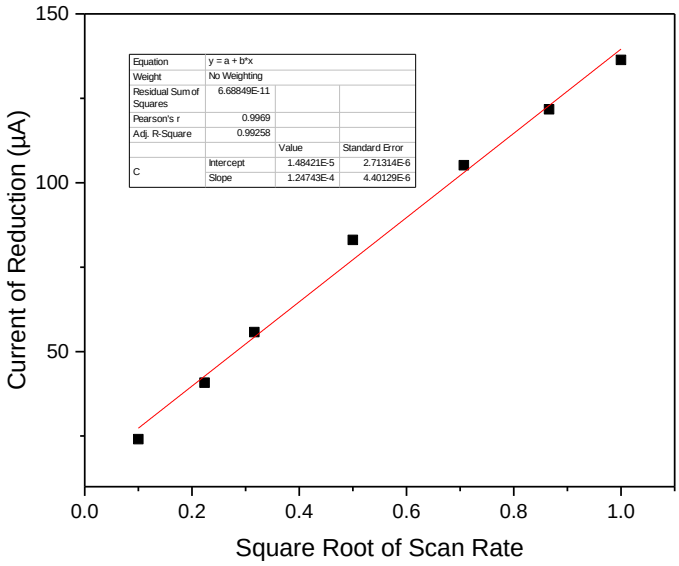

Figure 54: Scan rate dependence: Plot of reductive peak current in cyclic voltammograms from Figure 53 versus square root of scan rate. A linear fit is observed, consistent was a diffusional system.

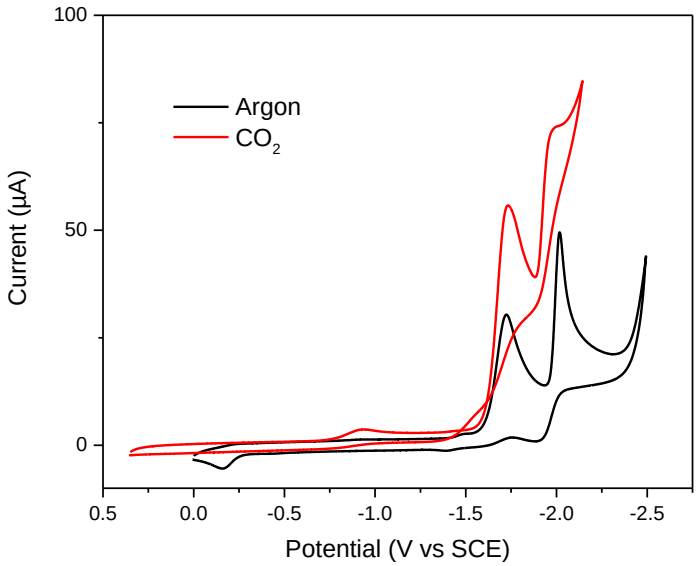

Figure 55: Cyclic voltammograms at 100 mV/s scan rate of 1 mM **4** under an argon and carbon dioxide atmosphere in 0.1 M $TBAPF_6$/MeCN. A glassy carbon working electrode was used with a platinum wire counter electrode. A platinum wire was also used as a quasi-reference electrode. Ferrocene was added at the end of experiments as an internal standard.

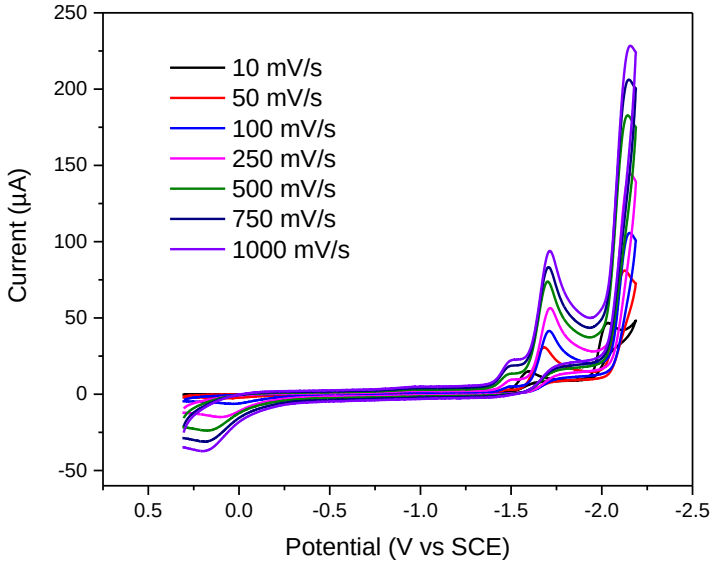

Figure 56: Cyclic voltammograms of 1 mM **4** under an argon atmosphere in 0.1 M $TBAPF_6$/MeCN with 1.1 M TFE added as a proton source. A glassy carbon working electrode was used with a platinum wire counter electrode. A platinum wire was also used as a quasi-reference electrode. Ferrocene was added at the end of experiments as an internal standard.

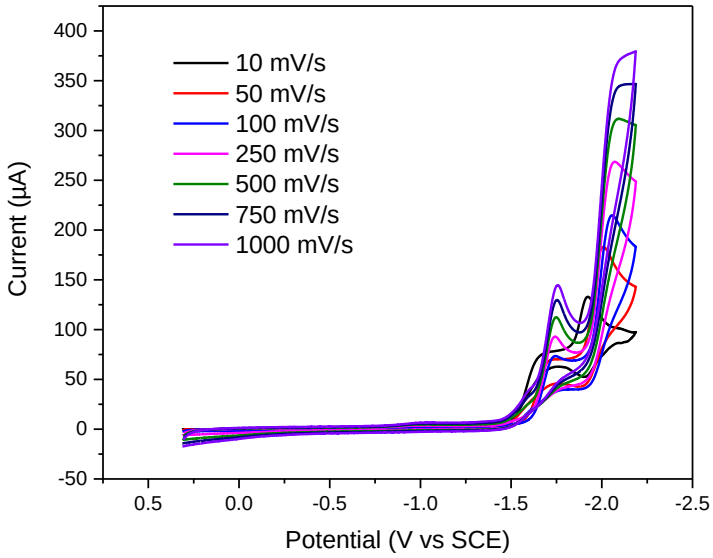

Figure 57: Cyclic voltammograms of 1 mM **4** under a carbon dioxide atmosphere in 0.1 M $TBAPF_6$/MeCN with 1.1 M TFE added as a proton source. A glassy carbon working electrode was used with a platinum wire counter electrode. A platinum wire was also used as a quasi-reference electrode. Ferrocene was added at the end of experiments as an internal standard.

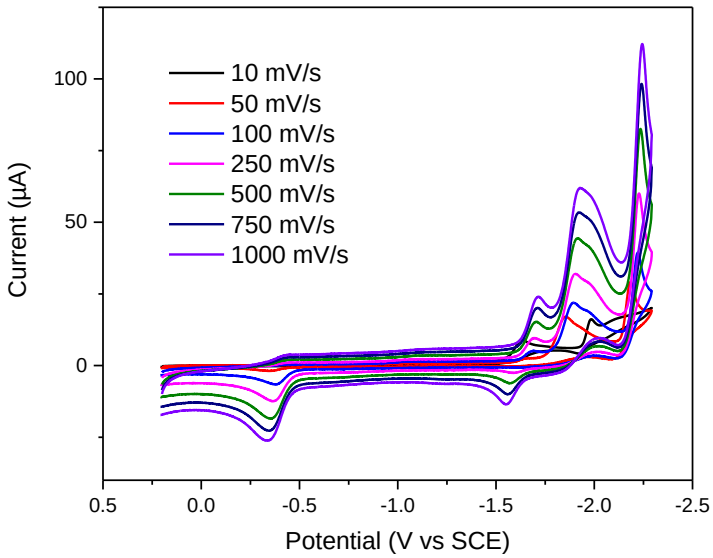

Figure 58: Cyclic voltammograms of 1 mM **4** under an argon atmosphere in 0.1 M $TBAPF_6$/MeCN with 2 M H_2O added as a proton source. A glassy carbon working electrode was used with a platinum wire counter electrode. A platinum wire was also used as a quasi-reference electrode. Ferrocene was added at the end of experiments as an internal standard.

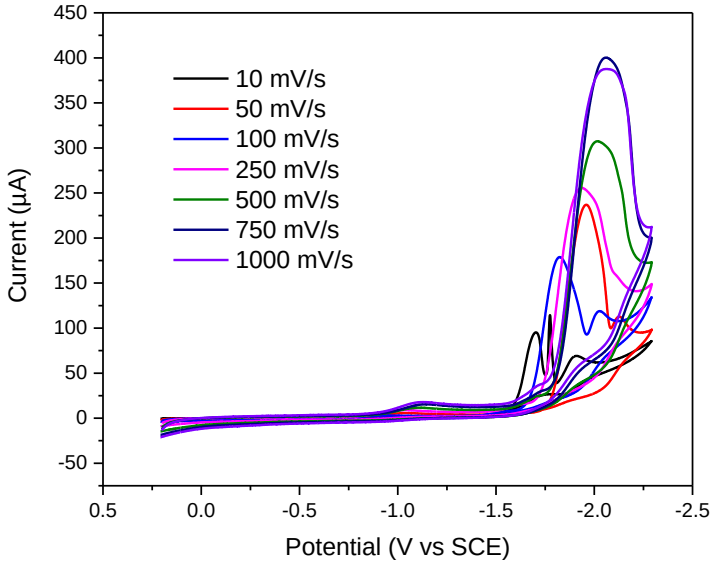

Figure 59: Cyclic voltammograms of 1 mM **4** under a carbon dioxide atmosphere in 0.1 M $TBAPF_6$/MeCN with 2 M H_2O added as a proton source. A glassy carbon working electrode was used with a platinum wire counter electrode. A platinum wire was also used as a quasi-reference electrode. Ferrocene was added at the end of experiments as an internal standard.

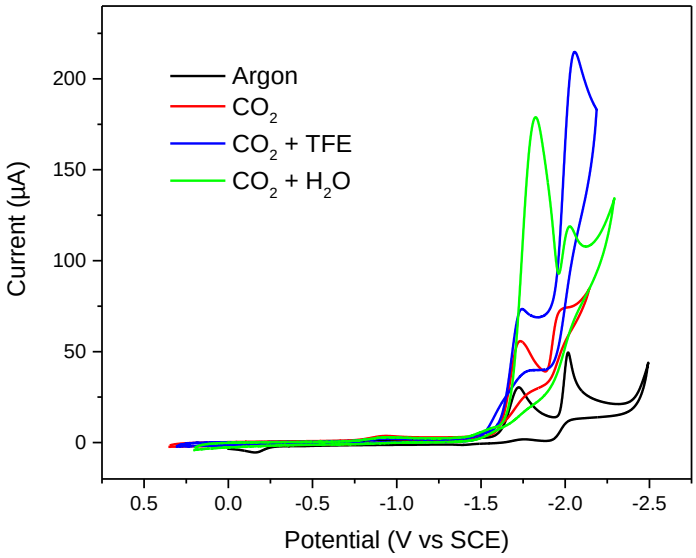

Figure 60: Cyclic voltammograms at 100 mV/s scan rate of 1 mM **4** under argon and carbon dioxide atmosphere in 0.1 M $TBAPF_6$/MeCN. TFE (1.1 M) and H_2O (2 M) were used as a proton source. A glassy carbon working electrode was used with a platinum wire counter electrode. A platinum wire was also used as a quasi-reference electrode. Ferrocene was added at the end of experiments as an internal standard.

Proton Source	[H^+]	$(i_{cat}/i_p)^2$ Peak 1	TOF (s^{-1}) Peak 1	$(i_{cat}/i_p)^2$ Peak 2	TOF (s^{-1}) Peak 2
None	—	3.3711	0.6534	2.2532	0.4367
TFE	1.1M	3.1324	0.6071	4.1256	0.7996
H_2O	2M	66.4711	12.8830	9.0790	1.7596

Table 6: All peak currents taken using 100mV/s scan rates. Tabulated Results of **4** utilizing various proton sources. These results were obtained from the cyclic voltammagrams shown above. The calculations for turnover frequency were done using the equation proposed by the Kubiak group.[45]

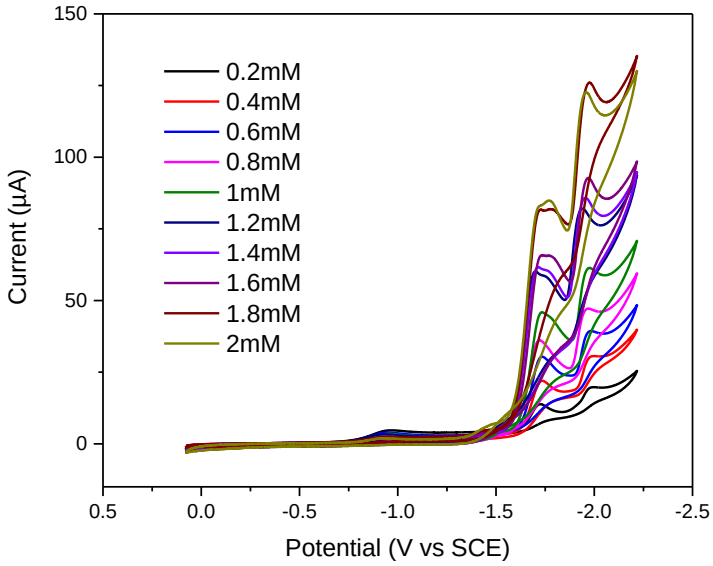

Figure 61: Cyclic voltammograms at 100 mV/s scan rate of **4** under a carbon dioxide atmosphere in 0.1 M $TBAPF_6$/MeCN. The [**4**] is changing from 0 to 2 mM. A glassy carbon working electrode

was used with a platinum wire counter electrode. A platinum wire was also used as a quasi-reference electrode. Ferrocene was added at the end of experiments as an internal standard.

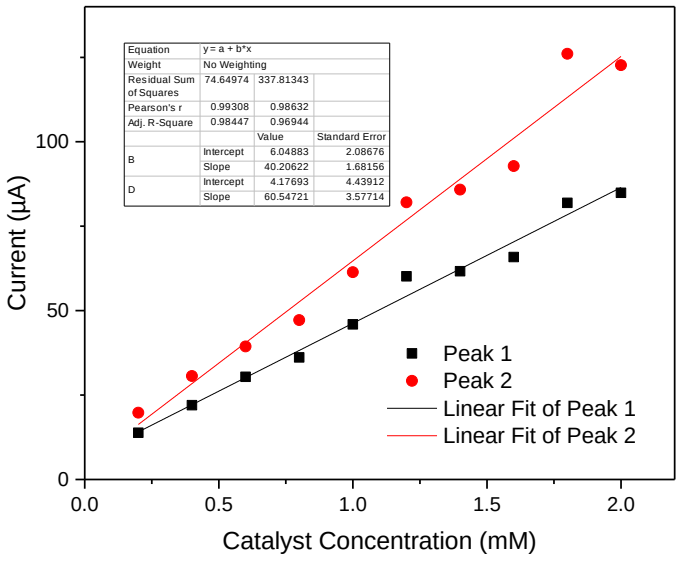

Figure 62: Plot of reductive peak current in cyclic voltammograms from Figure 61 as a function of the concentration of **4** under a carbon dioxide atmosphere in 0.1 M $TBAPF_6$/MeCN (scan rate = 100 mV/s). A linear fit at both the first and second reductions is consistent with catalysis that is first order with respect to catalyst.

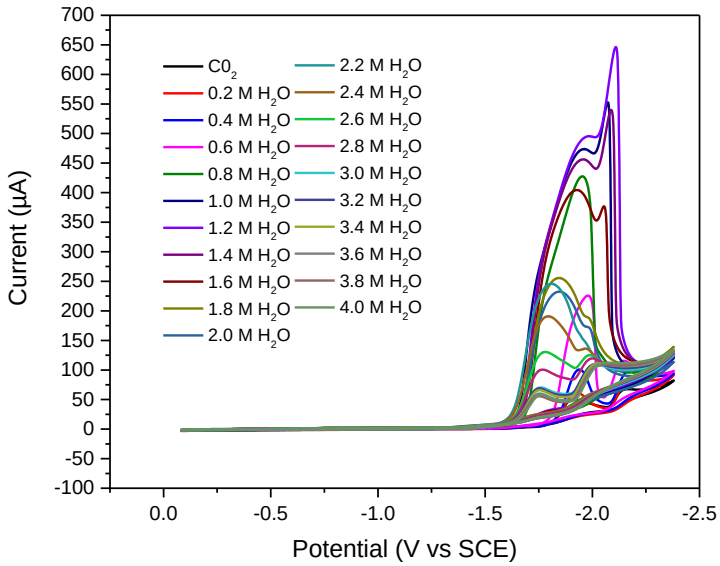

Figure 63: Cyclic voltammograms at 100 mV/s scan rate of 1 mM **4** under a carbon dioxide atmosphere in 0.1 M $TBAPF_6$/MeCN. The [H_2O] is changing from 0 to 4 M. A glassy carbon working electrode was used with a platinum wire counter electrode. A platinum wire was also used as a quasi-reference electrode. Ferrocene was added at the end of experiments as an internal standard.

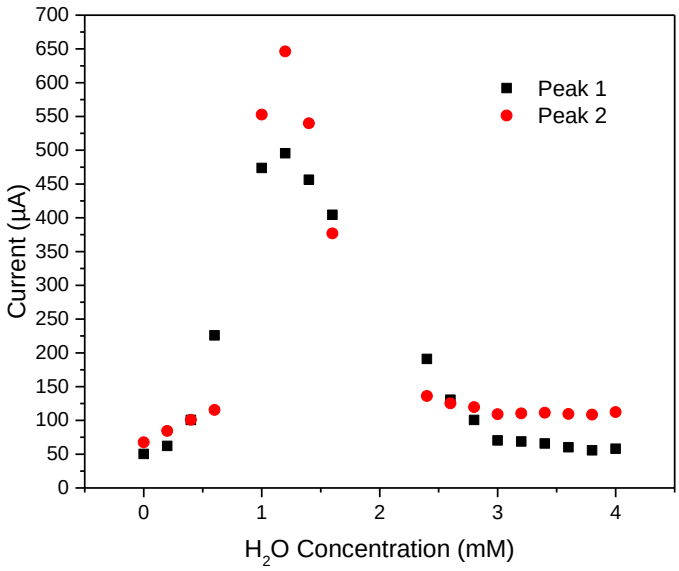

Figure 64: Plot of reductive peak current as a function of [H_2O] from the cyclic voltammograms in Figure 63. The scatter plot should form a linear increase with a plateau when plotted against the [H_2O]. This would show that the catalytic reaction is first order with regard to the proton source. The plot currently does not represent any form of dependence on the [H_2O].

Electrochemical studies were performed on **4** to test for its catalytic properties. The catalytic system was found to be diffusional, given the high R^2 value when the reduction potentials were plotted vs the square root of the scan rate. The catalyst showed mild activity under a catalytic atmosphere of carbon dioxide. This increase in current under the catalytic environment can be seen in comparison to the neutral environment in figure 55. The activity shown under the catalytic atmosphere makes it interesting for some further investigation.

The catalyst was also investigated with different common proton sources. A comparison of the catalyst with these proton sources under a catalytic environment and the catalyst under a non-catalytic environment. This comparison can be seen in figure 60. The catalyst shows some

change in activity when the proton source is introduced. It is interesting to note that H_2O increased the activity at the first reduction potential, while TFE increased the activity at the second reduction potential. The activity shown at the first reduction potential is novel for this series of catalysts and was the main cause for further investigation of the catalyst. Further investigation was done utilizing a gas chromatograph in order to discover the efficiency and selectivity of this catalyst, but it fell outside of the realm of my involvement in this collaboration.

A series of papers on this complex have been reported by Dr. Delcamp's group. The group has discussed synthesis of a variety of complexes and their properties, photochemical activity, and an electrochemical investigation. Future work is coming with this series of catalysts to investigate the tuning of reduction at the first reduction potential.[46-48]

CONCLUSION

Over the course of the previous two years, I have completed and optimized a synthetic procedure for a novel ligand, created and crystalized a nickel complex with the novel ligand that shows catalytic activity, and performed a number of electrochemical investigations for my own complex and other complexes that have been created by my colleagues within the department. The ligand synthesis and nickel complex have been reported for the first time for the presentation of this thesis. The nickel complex shows some moderate catalytic activity in the presence of a carbon dioxide environment. The results given here are preliminary results that offer a compelling argument for further investigation. The future studies will be conducted by fellow grad students and involve controlled potential electrolysis and the utilization of a gas chromatograph to quantify the efficiency and selectivity of the catalyst. My electrochemical investigations have led to one publication with Dr. Delcamp's group, and I feel confident that my research can contribute to numerous publications for Dr. Jurss' group in the near future.

BIBLIOGRAPHY

1. http://www.eia.gov/totalenergy/data/monthly/pdf/sec1_3.pdf
2. http://www.eia.gov/todayinenergy/detail.cfm?id=26212
3. http://www.un.org/en/development/desa/news/population/2015-report.html
4. https://www3.epa.gov/climatechange/science/causes.html
5. http://nca2014.globalchange.gov/
6. Lewis; Nocera; *Proc. Natl. Acad. Sci. USA* **2006**, *103*, 15729
7. Wigley TML, Richels R, Edmonds JA; *Nature* **1996**, *379*, 240–243.
8. Maier-Reimer E, Hasselmann K; *Climate Dyn* **1987**, *2*, 63–90.
9. Intergovernmental Panel on Climate Change; *Climate Change 2001, Synthesis Report Summary for Policymakers* (Intergovernmental Panel on Climate Change, Washington, DC), Third Assessment Report. **2001**
10. Geider, R. J.; *Global Change Biol.* **2001**, *7*, 849-882
11. Taiz, L.; Zeiger, E.; *Plant Physiology*; Fourth Edition; Sinauer Associates, Inc., **2006**
12. https://www.britannica.com/science/photosynthesis/The-pathway-of-electrons
13. http://www.life.illinois.edu/govindjee/ZSchemeG.html
14. *Campbell, Neil A.; Brad Williamson; Robin J. Heyden; Biology: Exploring Life. Boston, Massachusetts: Pearson Prentice Hall, **2006***
15. *Meyer; Energy Environ. Sci.* **2012**, *5*, 7704–7717
16. J. H. Alstrum-Acevedo, M. K. Brennaman, T. J. Meyer; *Inorg. Chem.* **2005**, *44*, 6802–6827.
17. W. Song, Z. Chen, M. K. Brennaman, J. J. Concepcion, A. T. Patrocinio, N. Y. Murakami Iha, T. J. Meyer; *Pure Appl. Chem.* **2011**, *83*, 749–768.
18. Love; *Chem. Commun.* **2012**, *48*, 1392

19. E. E. Benson, C. P. Kubiak, A. J. Sathrum, J. M. Smieja; *Chem. Soc. Rev.* **2009**, *38*, 89.

20. T. Sakakura, J.-C. Choi, H. Yasuda; *Chem. Rev.* **2007**, 107.

21. D. L. DuBois, *Encyclopedia of Electrochemistry* **2006**, *7a*, 202

22. J. M. Saveant, *Chem. Rev.* **2008**, *108*, 2348

23. H. Schulz; *Advance Catalysis*, **1999**, *186*, 3-12

24. Kubiak; *Inorg. Chem.* **2012**, *51*, 3932

25. Beley, M.; Collin, J.-P.; Ruppert, R.; Sauvage, J. P.; *J. Chem. Soc., Chem. Commun.* **1984**, 1315

26. Beley, M.; Collin, J. P.; Ruppert, R.; Sauvage, J. P.; *J. Am. Chem. Soc.* **1986**, *108*, 7461

27. Kubiak; *J. Am. Chem. Soc.* **2015**, *137*, 3565−3573

28. Fisher, B. J.; Eisenberg, R.; *J. Am. Chem. Soc.* **1980**, *102*, 7361

29. Schneider, J.; Jia, H.; Kobiro, K.; Cabelli, D. E.; Muckerman, J. T.; Fujita, E.; *Energy Environ. Sci.* **2012**, *5*, 9502

30. Balazs, G. B.; Anson, F. C.; *J. Electroanal. Chem.* **1992**, *322*, 325

31. http://shrinkthatfootprint.com/shrink-your-housing-footprint

32. World Energy Council (2004) *Comparison of Energy Systems Using Life Cycle Assessment*

33. Zilbermann, I.; Winnik, M.; Sagiv, D.; Rotman, A.; Cohen, H.; Meyerstein, D.; *Inorg. Chem. Acta* **1995**, *240*, 503

34. Bujno, K.; Bilewicz, R.; Siegfried, L.; Kaden, T. A.; *J. Electroanal. Chem.* **1998**, *445*, 47

35. Kujihira, M.; Hirata, Y.; Suga, K.; *J. Electroanal. Chem.* **1990**, *292*, 199.

36. Connolly, P. J.; Billo, E.; *J. Inorg. Chem.* **1987**, *26*, 3224

37. Chang; *Chem. Commun.* **2011**, *47*, 6578

38. E. E. Benson, C. P. Kubiak, A. J. Sathrum and J. M. Smieja, *Chem. Soc. Rev.* **2009**, *38*, 89–99.

39. Chang; *J. Am. Chem. Soc.* **2013**, *135*, 14413

40. Ma, H.-C.; Jiang, X.-Z. *J. Org. Chem.* **2007**, *72*, 8943

41. Z. Xi, X. Zhang, W. Chen, S. Fu and D. Wang, *Organometallics* **2007**, *26*, 6636–6642.

42. Xi, Z.; Zhang, X.; Chen, W.; Fu, S.; Wang, D. *Organometallics* **2007**, *26*, 6636.

43. Zhou, Y.; Xi, Z.; Chen, W.; Wang, D. *Organometallics* **2008**, *27*, 5911

44. Gu, S.; Chen, W. *Organometallics* **2009**, *28*, 909.

45. Kubiak; *Inorg. Chem.* **2013**, *52*, 2484-2491

46. Delcamp; *Inorg. Chem.* **2016**, *55*, 6085−6094

47. Huckaba, A. J.; Sharpe, E. A.; Delcamp, J. H. *Inorg. Chem.* **2016**, *55*, 682.

48. Jupally, V. R.; Dharmaratne, A. C.; Crasto, D.; Huckaba, A. J.; Kumara, C.; Nimmala, P. R.; Kothalawala, N.; Delcamp, J. H.; Dass, A. *Chem. Commun.* **2014**, *50*, 9895

49. Wolf; *Synlett* **2012**, *23*, 1240

50. Li; *Adv. Synth. Catal.* **2009**, *351*, 2071

51. Keith; *J. Org. Chem.* **2008**, *73*, 327

52. Allam; *Appl. Mater. Interfaces* **2012**, *4*, 4413−4418

53. Kuhn; ***Catal. Sci. Technol.* 2014**,***4***, 3845-3849

54. Johannes; *Beilstein J. Org. Chem.* **2012,** *8*, 1037–1047

55. K. Inamoto, J.-i. Kuroda, K. Hiroya, Y. Noda, M. Watanabe and T. Sakamoto, *Organometallics*, 2006, **25**, 3095-3098

VITA

HUNTER DULANEY

EDUCATION

B.A. Biochemistry, University of Mississippi, August 2014

TEACHING EXPERIENCE

Teaching Assistant, 2012-2016

University of Mississippi

Course: General and Organic Chemistry

PUBLICATIONS

Dulaney, H. A.; *Inorg. Chem.* **2016**, *55*, 6085−6094